PNE-608F
FINAL REPORT

Plowshare / peaceful uses for nuclear explosives

UNITED STATES ATOMIC ENERGY COMMISSION / PLOWSHARE PROGRAM

project DUGOUT

NEVADA TEST SITE — JUNE 24, 1964

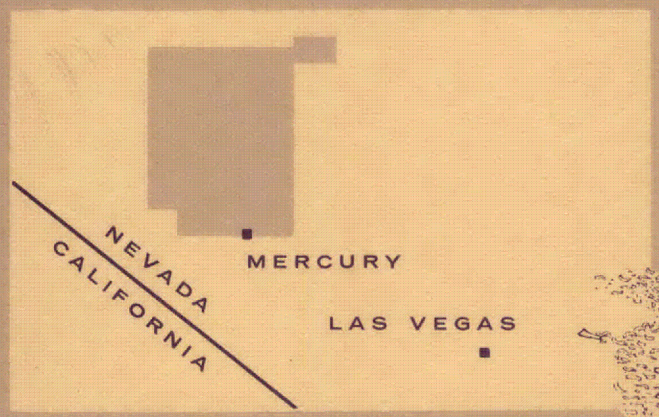

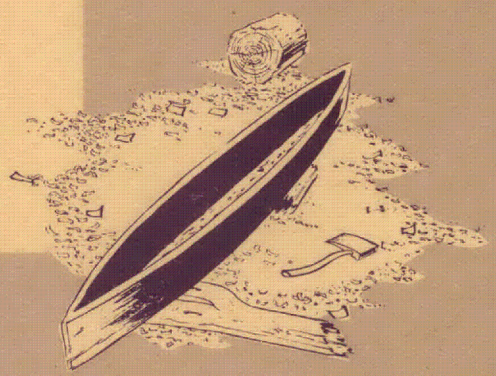

Close-in Air Blast From a Row Charge in Basalt

L. J. Vortman

Sandia Corporation

Issuance Date: August 4, 1965

LEGAL NOTICE

Printed in USA. Price $3.00. Available from the Clearinghouse for Federal Scientific and Technical Information, National Bureau of Standards, U. S. Department of Commerce, Springfield, Va.

USAEC Division of Technical Information Extension, Oak Ridge, Tennessee

PROJECT DUGOUT

PNE-608F

NUCLEAR EXPLOSIONS — PEACEFUL APPLICATIONS (TID - 4500, 43rd. Ed.)

CLOSE-IN AIR BLAST FROM A ROW CHARGE IN BASALT

L. J. Vortman

Sandia Corporation
Albuquerque, New Mexico

May 1965

ABSTRACT

Close-in air blast measurements were made on the Dugout shot (a row of five 18,000-kg high-explosive charges placed 17.9 meters below the surface in basalt). Major constituents of the blast wave were the ground-shock-induced pulse and the pulse from venting gases. The ground-shock-induced pulse was the dominant one at all stations. The pulse from venting gases was superimposed on the negative phase following the ground-shock-induced pulse; as a result, the positive pressures were less than they otherwise would have been. The ground-shock-induced overpressures perpendicular to the row were slightly more than twice those along the axis of the row. Perpendicular to the row, they were 3.3 times single charge values but only 1.4 times single charge values off the end of the row.

A third constituent of the blast wave precedes the ground-shock-induced pulse. Its timing indicates it is associated with a seismic wave. A subsequent experiment has shown that air pressure induced by the ground wave was measured.

Issued by Sandia Corporation,
a prime contractor to the
United States Atomic Energy Commission

FOREWORD

"This document is the author's report to the Technical Director of Project Dugout. The findings and conclusions contained herein are those of the author and are not necessarily those of the Atomic Energy Commission. Accordingly, references to this material must cite the author."

ACKNOWLEDGMENTS

The air-blast measurements were made by A. M. Triest, assisted by C. Csinnjinni, B. C. Holt, and K. B. Kimball. The measurements are the finest portrayals of wave shape at these low-pressure levels of which the author is aware. J. L. Martinez reduced the data, and the playbacks presented herein were done by D. B. Hayes and J. P. Dietz. Having overlooked the obvious for longer than he likes to realize, the author thanks M. D. Nordyke for pointing out an inconsistency in arrival times which led to proper identification of the various portions of the blast wave.

TABLE OF CONTENTS

CLOSE-IN AIR BLAST
FROM A ROW CHARGE IN BASALT

CH 1 - INTRODUCTION

1.1 Description of Dugout Event

Project Dugout was a chemical row-charge cratering experiment in hard rock executed as part of the Plowshare Program for development of nuclear excavation. The purpose of the experiment was to develop a more complete understanding of the fundamental processes involved in row-charge cratering.

Dugout was fired June 24, 1964, at approximately 0806 Pacific Daylight Time (1506 Greenwich Mean Time). Five separately placed 20 ± 1.5 ton (18,000 kg) charges were fired simultaneously. The explosive used was liquid nitromethane contained in a mined spherical cavity approximately 10.3 feet (3.14 m) in diameter. The center of the cavities was at a depth of 58.8 ± 0.2 feet (17.9 m). The holes were spaced 45 feet (13.7 m) apart.

Emplacement hole U18i, the center hole in the array, was located at geodetic coordinates

Lat.	37°	5'	37.8381"
Long.	116°	20'	39.3410"

The elevation and Holmes and Narver grid coordinates of the entire array were as follows:

Hole	Collar Elevation	Collar Coordinates
U18g	5384.56 ft (1641.44 m)	N 853,289.90 E 594,120.20
U18h	5385.45 ft (1641.49 m)	N 853,290.00 E 594,075.00
U18i	5386.51 ft (1641.81 m)	N 853,289.94 E 594,030.06
U18j	5386.90 ft (1641.93 m)	N 853,290.00 E 593,985.12
U18k	5387.50 ft (1642.11 m)	N 853,290.10 E 593,940.00

1.2 Objectives

The objectives of this investigation were

1. To measure air blast as a function of distance both normal and parallel to a row-charge explosion at near-optimum cratering depth in hard rock, and

2. To lay the foundation for predicting blast from large-yield nuclear row-charge explosions by:

   a. comparing results with single-charge explosions in the same medium, and

   b. establishing blast suppression for charge burial.

1.3 Background

Blast waves have been examined in the past from above-ground detonation of infinite-line charges[1] and horizontal-cylindrical charges (short-line charges).[2] Experimental work[3] on the former considered only blast along the axis perpendicular to the long axis of the charge. For the horizontal-cylindrical charges (L/D = 2), the ratio of peak pressures perpendicular to the charge axis to that along it increased with ground range as follows:

Scaled Range ($m/kg^{1/3}$)	$P_{\perp}/P_{\parallel}$
3.77	1.15
4.85	1.19
6.46	1.43

Ratios of a positive-phase impulse perpendicular to the axis to that along the axis exhibited a decreasing trend with distance:

Scaled Range ($m/kg^{1/3}$)	$I_{\perp}/I_{\parallel}$
3.77	1.14
4.85	1.03
6.46	1.00
8.61	0.95

Each cylinder was detonated at both ends.

No information is available on air blast from rows of charges detonated above ground. Where such charges are sufficiently close together and detonated simultaneously, the air blast is equivalent to that from a line charge of a weight per unit length, W/S, where W is the weight of each charge in the row and S is the spacing between charges. Thus, the short cylinders cited above could represent a row of two charges spaced very closely together. To be comparable with simultaneously detonated row charges, a line charge

must have an infinite detonation velocity or be simultaneously initiated once per unit length S.

Air blast from single HE charges buried at or near the depth which maximizes crater dimensions has a typical waveform shown in Figure 1.1. The ground-shock-induced wave originates when the ground directly over the charge pulses the adjacent air. From the region of the epicenter, the wave propagates with the appropriate velocity in air. The waveform shown in the figure was that obtained from Scooter[4] and is typical of the Stagecoach[5] shot at a 34.2-foot burial depth in alluvium. In the case of Scooter, both the ground-shock-induced and the wave from venting gases propagated at essentially the same velocity, i.e., 341.5 m/sec. Velocities of both waves were equal for the Stagecoach shot but were different from those of Scooter. No arrival time information was obtained from the three Buckboard[6] 18,144-kg high-explosive detonations in the same basalt as Dugout. The blast wave from a simultaneously detonated row charge would be expected to have a similar form, especially perpendicular to the axis of the row. Along the axis, however, contributions from the ground shock of individual charges could become apparent if the spacing was large and ground-shock velocity small.

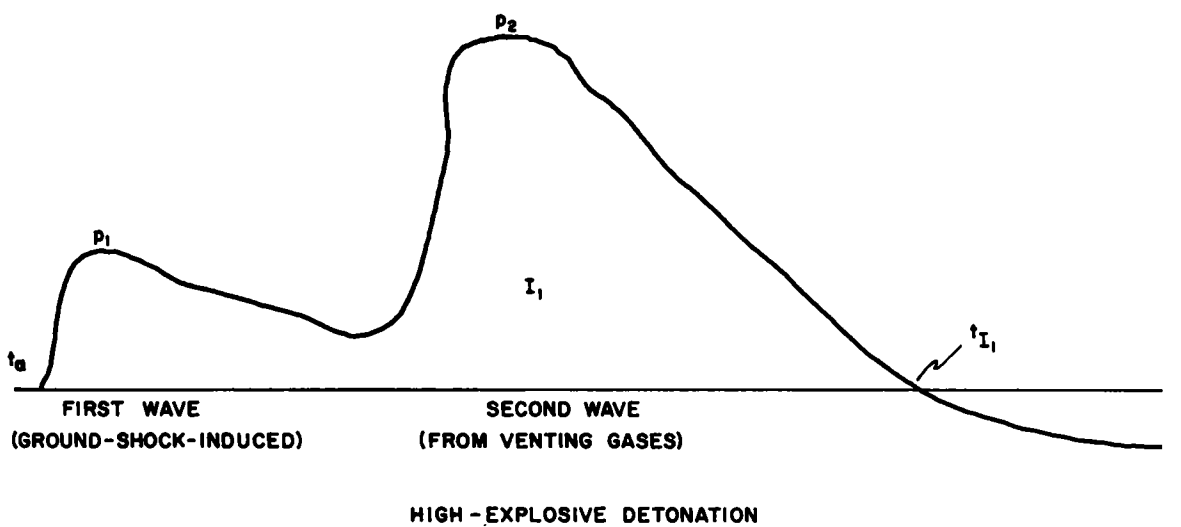

Figure 1.1. Typical air-blast pressure waveform from single charges

Information is available[7] on only one simultaneously detonated row-charge experiment. On this experiment, data were obtained parallel and perpendicular to a row of eleven 3.63-kg, spherical-cast, TNT charges detonated simultaneously. No difference in attenuation of peak pressure with distance from that of single charges was discerned. No information was obtained on positive-phase impulse and positive-phase duration. No measurements were made on blast from single 3.63-kg charges. However, peak pressures can be inferred by scaling data from other sizes of single charges fired at comparable scaled burial depths (0.58 $m/kg^{1/3}$) in other media. Such a comparison shows the relationship of peak overpressure from a single charge to that from one end

of the 11-charge row (measured from the end charge) and to that along a line perpendicular to the row (measured from the center charge in the row). Averages of two 11-charge shots suggested that peak overpressure along the axis of the row was about 80 percent greater than it would have been at the same distance from one of the charges. Perpendicular to the axis, the peak overpressure was 5-1/4 times that to be expected from a single charge at the same distance, i.e., about one-half the product of single-charge peak overpressure and the number of charges. Thus, peak overpressures normal to the row were nearly three times those off the ends.

Although row-charge cratering experiments employing charges larger than 3.63 kg have been made at the Nevada Test Site,[8,9,10] no air-blast measurements were made.

Air-blast measurements were made on a single 18,000-kg high-explosive charge[6] (Project Buckboard Shot 13), which is equal to one of the charges in the Dugout row, at the same scaled burial depth as Dugout and in the same medium. These results, which are reproduced in Appendix A as Figures A.1, A.2, A.3, A.4, and A.5, constitute the single-charge standard against which the row-charge results can be evaluated. One pressure-distance curve (Figure A.2) uses only the close-in data, while the other (Figure A.3) uses distant measurements in addition to those made close in.

CH 2 - PROCEDURE

2.1 Experimental Plan

Two blast lines were installed--one westward along the axis of the row and one southward perpendicular to the row. (Throughout the text, the terms "west" and "parallel" are used synonymously, as are "south" and "perpendicular," to describe the blast lines.)

Station locations (plotted in Figure 2.1) and the number of gages at each station were as follows:

South from Center Charge		West from End Charge	
Distance (m)	Number	Distance (m)	Number
51.8	2	51.8	2
107.0	2	108	2
259	2	259	2
		460	1
701	2	701	2
		1039	1
1522	2	1402	2

The additional stations along the west line coincided with a topographic peak (at a range of 460 m) and with its leeward valley (at 1039 m) and were included to determine if terrain perturbations on blast-wave propagation or shape were observable.

Expected overpressures for gage set ranges along each blast line were obtained in the following manner. An overpressure (5.3 millibars at 660 m) was chosen from Buckboard Shot 13 as a basis. Assuming $p \sim R^{-1}$, the overpressures so described were multiplied by 1.4 for the west (parallel) line and 2.5 for the south (perpendicular) line. These values are about half those obtained on the earlier high-explosive experiment, since Dugout involved about half as many charges. An additional factor was then applied to accommodate unexpected overpressures to prevent overranging the gages; this pressure was then rounded to a convenient figure.

In terms of overpressures producing damage the range covered by the measurements may seem large, and the expected pressures may seem small. However, if these results were to be extrapolated to a row of 10-megaton nuclear charges (9×10^9 kg TNT equivalent), the distances would range from 4.1 km (2.5 miles) to 121 km (75 miles). In such a full-scale explosion, meteorology would greatly modify the blast propagation. This experiment, however, provides information for a model approaching that for a homogeneous stationary atmosphere on which the model for a nonhomogeneous dynamic atmosphere may be based.

2.2 Instrumentation

Pace P-7 diaphragm-type pressure gages were used. Information was carried through Consolidated System D amplifiers with an 800-cps response to an Ampex CP-100 magnetic tape recording system.

In measuring peak overpressures of a few millibars, the major gage problem is calibration. The Pace gages are calibrated using a slant-tube water manometer. In addition, the gage is sufficiently sensitive to dust on and around the diaphragm that cleaning is necessary after each use. Both calibration and dust may be responsible for some of the irregularities discussed in Chapter 4. The gages gave excellent portrayals of the wave shapes although amplitude accuracies often left much to be desired.

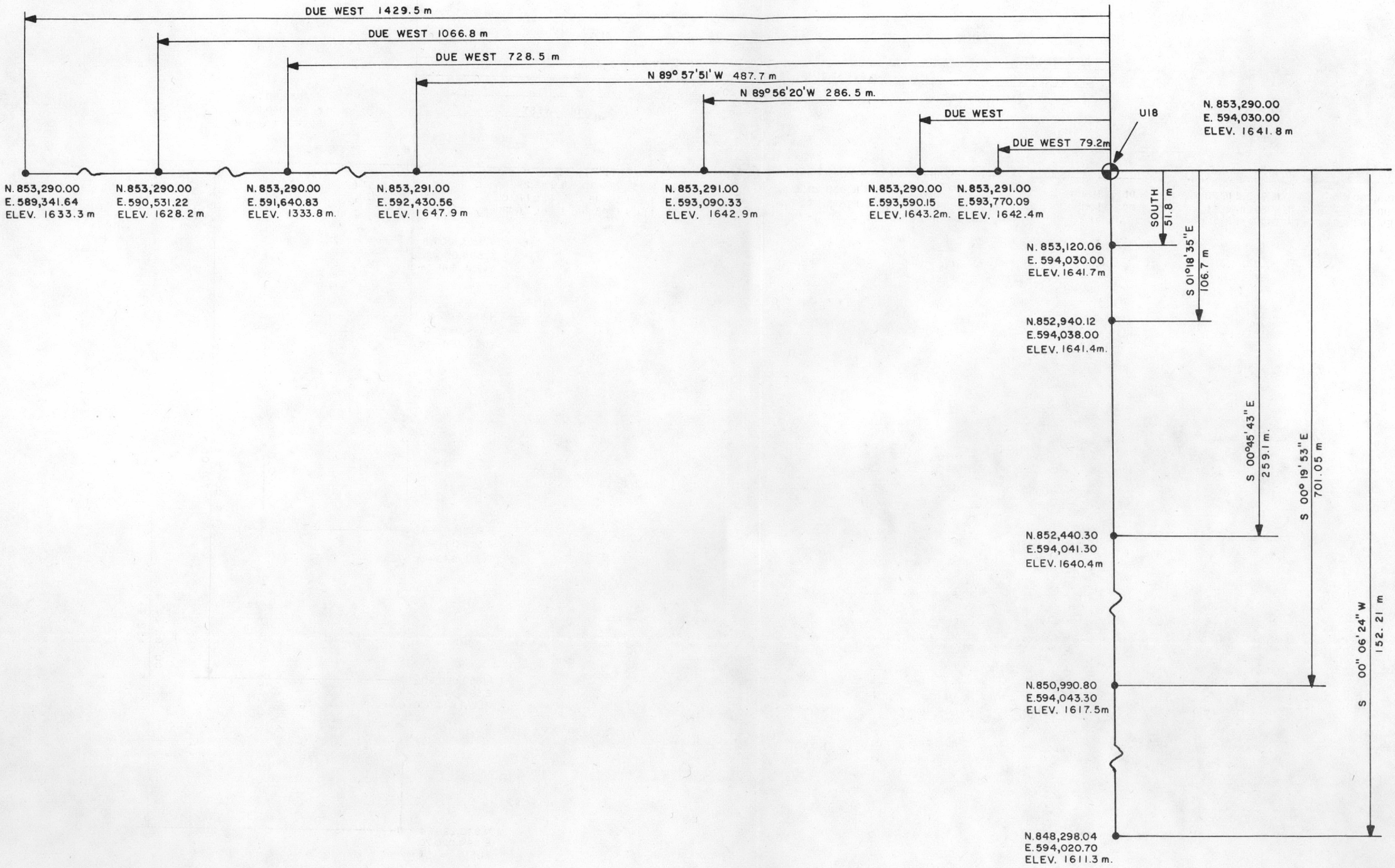

Figure 2.1. Station locations

CH 3 - TEST RESULTS

3.1 Summary of Results

Table 3.1 summarizes the results of the pressure measurements. The column headings of Table 3.1 are defined by Figure 3.1. Pressure records are reproduced in Figures 3.2 to 3.7. The records are complete with the exception of those from the station at 1522 m on the south line. At this station, a signal from a nearby microbarograph calibration charge arrived at about 6 seconds and interfered with the balance of the record.

The results are considered quite good especially in view of the low overpressures being measured. Certain exceptions occur, the most notable being the record of gage S701-1 (i.e., gage 1 at station 701 meters south of shot) which is consistently high by nearly a factor of five. A human error in recording attenuator settings is suspected. Other exceptions were records of gages S107-1, S1522-2, W460-1, W701-1, W701-2, W1402-1, and W1402-2, which appear to give values which are high with respect to other records, and the record of gage W1402-2, which appears low. These departures from expected pressures are discussed in Chapter 4.

3.2 Wave Shape

Figure 3.1 illustrates the typical Dugout wave shape. The most remarkable feature of the shape is the positive and negative phases subsequent to the first. Ordinarily, for single charges, a single positive phase is followed by a single negative pulse. For the shot of eleven 3.63-kg charges referred to above, a second positive pulse was prominent but no subsequent waves could be detected.

3.3 Arrival Times

Time of arrival data are plotted in Figures 3.8 and 3.9.

3.4 Pressure, Impulse, and Duration

Principal data for pressures, impulses, and durations are plotted in Figures 3.10 through 3.13. Auxiliary data are plotted in Figures A.6 through A.13 in the appendix. The pressure-distance relation for a nuclear free air burst of a single charge comparable to the total charge weight was scaled from IBM Problem M and added to Figure 3.11 for comparison.

TABLE 3.1

Dugout Pressure Measurements

Gage	t_a (sec)	p_1 (mbar)	t_{p_1} (sec)	p_2 (mbar)	t_{p_2} (sec)	I_1 (mbar-sec)	t_{I_1} (sec)	p_{-1} (mbar)	$t_{p_{-1}}$ (sec)	I_{-1} (mbar-sec)	$t_{I_{-1}}$ (sec)
S51.8-1	0.0245	19.41	0.041	30.26	0.157	3.29	0.287	-3.86	0.335	0.441	0.509
-2	0.0245	17.30	0.038	25.82	0.172	3.04	0.308	-1.25	0.353	0.0469	0.385
S107-1	0.0535	1.59	0.062	7.99	0.313	0.961	0.471	-0.700	0.507	0.0304	0.657
-2	0.054	2.54	0.065	11.52	0.313	1.36	0.477	-0.975	0.515	0.0566	0.590
S259-1	0.197	0.261	0.208	5.72	0.754	0.544	0.991	-0.599	1.047	0.0483	1.132
-2	0.1845	0.303	0.204	5.77	0.753	0.589	0.989	-0.543	1.047	0.0386	1.130
S701-1	0.439	0.376	0.478	6.91	2.049	0.786	2.306	-0.403	2.342	0.0186	2.390
-2	0.436	0.097	0.471	1.42	2.048	0.208	2.317	-0.057	2.352	0.00207	2.380
S1522-1				0.589	4.430	0.0704	4.686	-0.048	4.740	0.00276	4.797
-2	4.119*			0.451	4.432	0.0538	4.677	-0.048	4.760	0.00207	4.797
W51.8-1	0.0295	7.03	0.056	12.00	0.145	2.15	0.392	-2.45	0.546	0.277	0.593
-2	0.0275	6.48	0.055	10.77	0.145	2.04	0.398	-2.19	0.535	0.243	0.590
W108-1	0.0565	0.493	0.064	5.25	0.310	0.952	0.547	-0.702	0.621	0.0635	0.723
-2	0.0575	0.651	0.061	4.62	0.308	0.876	0.550	-0.861	0.623	0.0697	0.725
W259-1	0.169	0.08	0.174	1.95	0.865	0.342	0.987	-0.482	1.131	0.0580	1.205
-2	0.145	0.170	0.204	1.50	0.878	0.264	0.983	-0.369	1.135	0.0449	1.201
W460-1	0.345	0.079	0.365	1.57	1.442	0.310	1.589	-0.232	1.696	0.0179	1.763
W701-1	0.514	0.119	0.580	1.04	2.135	0.213	2.343	-0.206	2.398	0.0124	2.463
-2	~0.529	0.109	0.567	0.844	2.136	0.173	2.345	-0.153	2.402	0.0159	2.458
W1039-1	0.601	0.031	0.622	0.398	3.113	0.0759	3.279	-0.079	3.361	0.00759	3.436
W1402-1				0.527	4.057	0.103	4.196	-0.091	4.297	0.0069	4.382
-2				0.116	4.053	0.0207	4.172	-0.028	4.309	0.00138	4.382

*Arrival of second pulse. First wave not discernible.

TABLE 3.1 (cont)

Gage	p_3 (mbar)	t_{p_3} (sec)	I_2 (mbar-sec)	t_{I_2} (sec)	p_{-2} (mbar)	$t_{p_{-2}}$ (sec)	I_{-2} (mbar-sec)	$t_{I_{-2}}$ (sec)	p_4 (mbar)	t_{p_4} (sec)	I_3 (mbar-sec)	t_{I_3} (sec)
S51.8-1	10.70	0.837	2.43	0.938	-8.99	1.379	5.86	2.039	4.91	2.390		
-2	8.90	0.800	2.61	0.966	-4.44	1.433	2.43	1.904	5.52	2.392		
S107-1	2.82	0.892	0.727	1.082	-3.12	1.569	2.16	2.191	1.75	2.527	0.685	~3.030
-2	4.13	0.908	1.05	1.081	-5.04	1.515	3.40	2.184	2.58	2.491	1.07	~3.089
S259-1	1.58	1.301	0.364	1.497	-2.24	1.957	1.53	2.613	1.02	2.932	0.375	3.322
-2	1.67	1.295	0.393	1.505	-2.16	1.984	1.44	2.588	1.10	2.905	0.453	3.359
S701-1	2.06	2.553	0.607	2.826	-2.80	3.323	1.85	3.957	1.31	4.228	0.498	4.765
-2	0.456	2.579	0.130	2.832	-0.587	3.251	--	--	--	--		--
S1522-1	0.204	4.926	0.0497	5.201	-0.259	5.651		Signal from microbarograph charge arrived				
-2	0.168	4.922	0.0386	5.207	-0.240	5.660		before crossover				
W51.8-1	4.82	0.730	1.17	0.949	-7.64	1.499	5.64	2.106	3.29	2.359	0.597	2.822
-2	4.34	0.729	1.07	0.956	-7.03	1.407	5.20	2.110	3.07	2.418	1.06	2.873
W108-1	2.48	0.982	0.613	1.131	-2.72	1.646	1.95	2.269	1.35	2.523	0.540	2.995
-2	2.40	0.978	0.586	1.132	-3.22	1.620	2.29	2.261	1.42	2.543	0.569	3.006
W259-1	0.851	1.406	0.159	1.552	-1.41	2.049	1.03	2.691	0.589	2.953	0.228	3.443
-2	0.693	1.411	0.126	1.549	-1.04	2.099	0.790	2.686	0.468	2.930	0.200	3.447
W460-1	0.842	1.989	0.186	2.154	-1.10	2.651	0.757	3.257	0.473	3.510	0.210	4.027
W701-1	0.580	2.690	0.144	2.864	-0.731	3.324	0.513	3.977	0.301	4.230	0.125	4.724
-2	0.473	2.687	0.118	2.860	-0.560	3.301	0.400	3.986	0.230	4.232	0.0987	4.730
W1039-1	0.215	3.662	0.0628	3.828	-0.278	4.325	0.184	4.934	0.135	5.170	0.0559	5.687
W1402-1	0.308	4.609	0.0614	4.765	-0.364	5.127	0.250	5.822	0.188	6.202	0.0828	6.611
-2	0.068	4.602	0.0124	4.751	-0.083	5.110	0.0538	5.824	0.044	6.123		

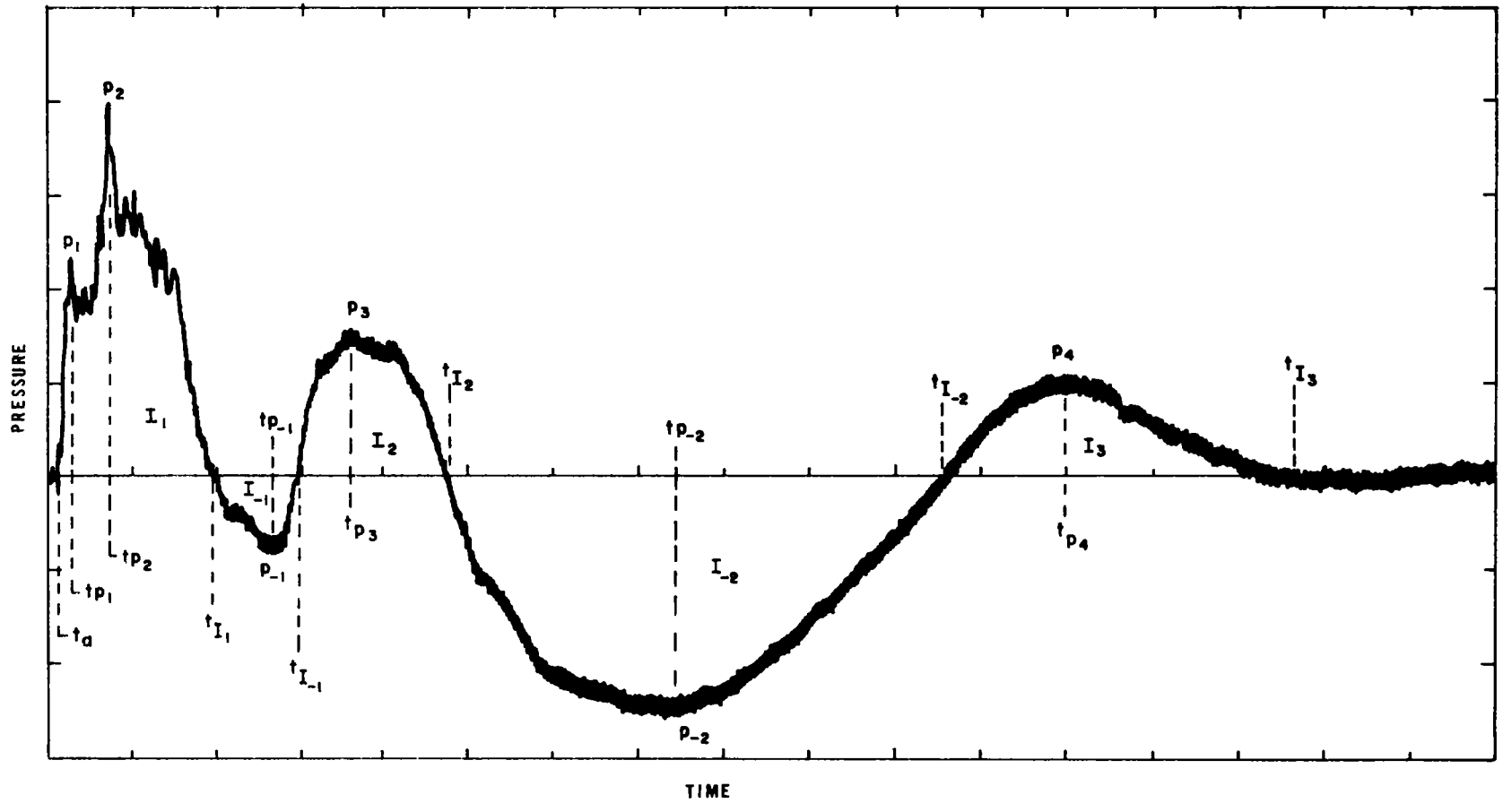

Figure 3.1. Definition of events in Dugout pressure records

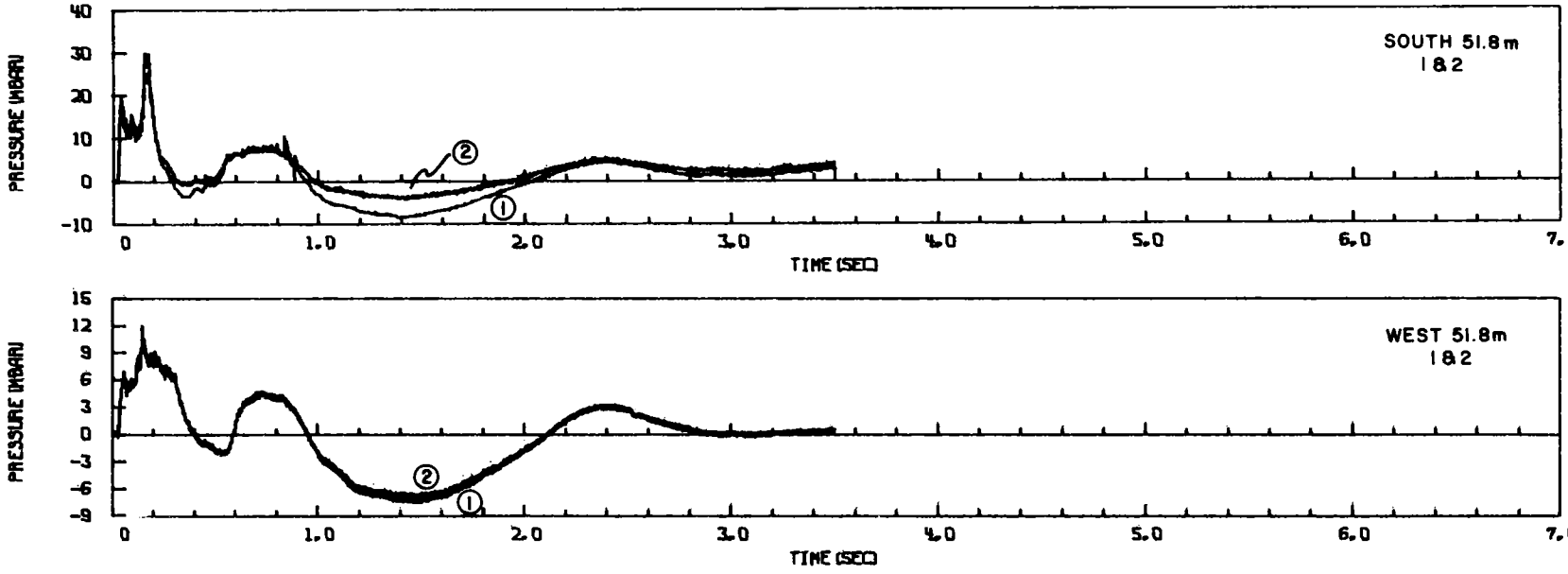

Figure 3.2. Pressure record--S51.8 and W51.8

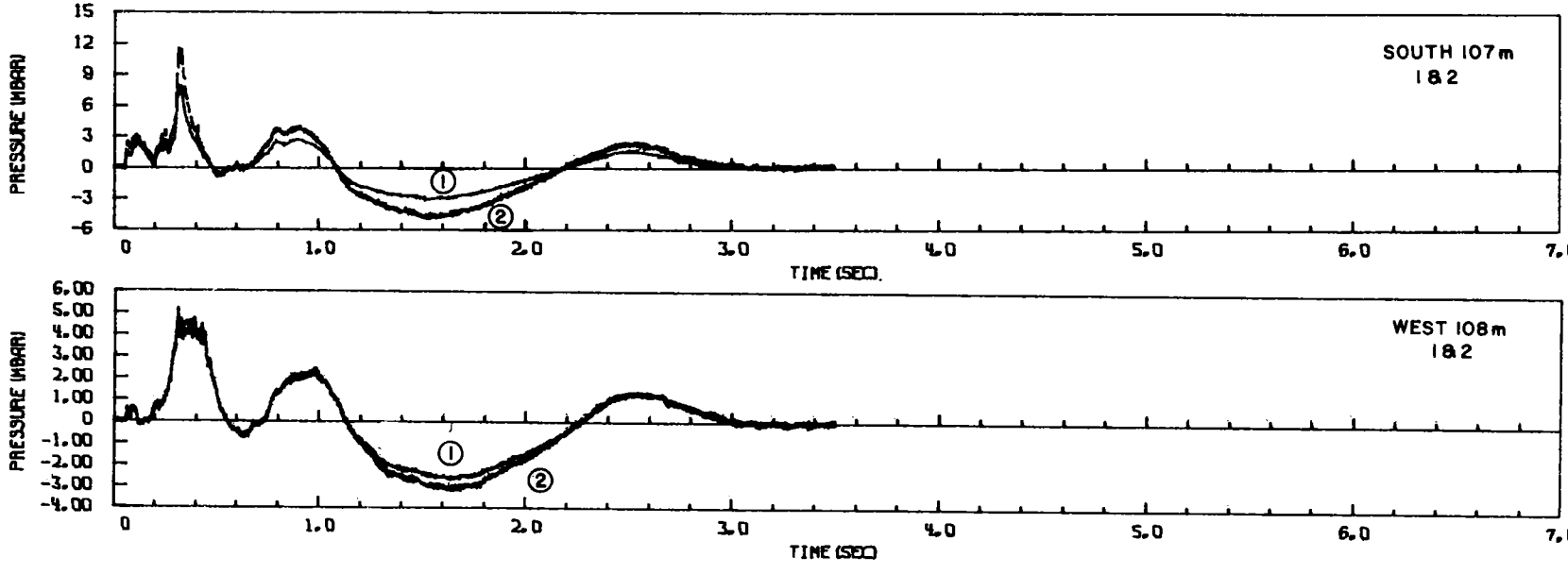

Figure 3.3. Pressure record--S107 and W108

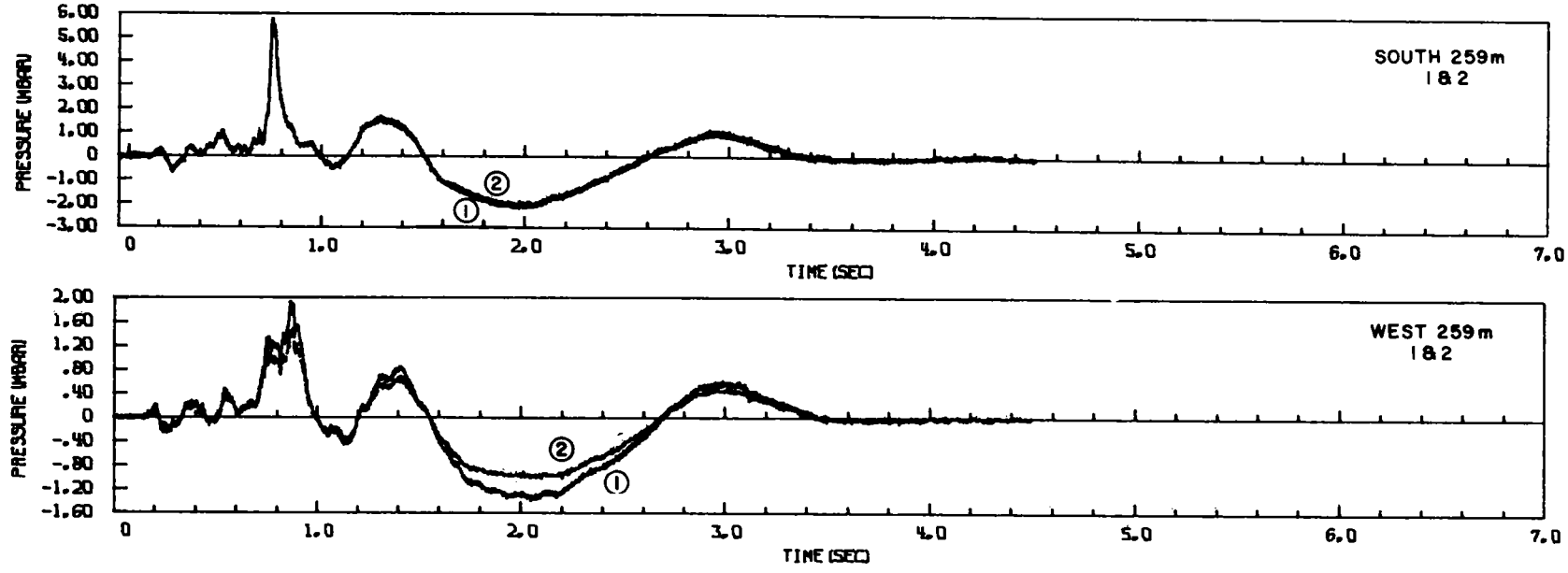

Figure 3.4. Pressure record--S259 and W259

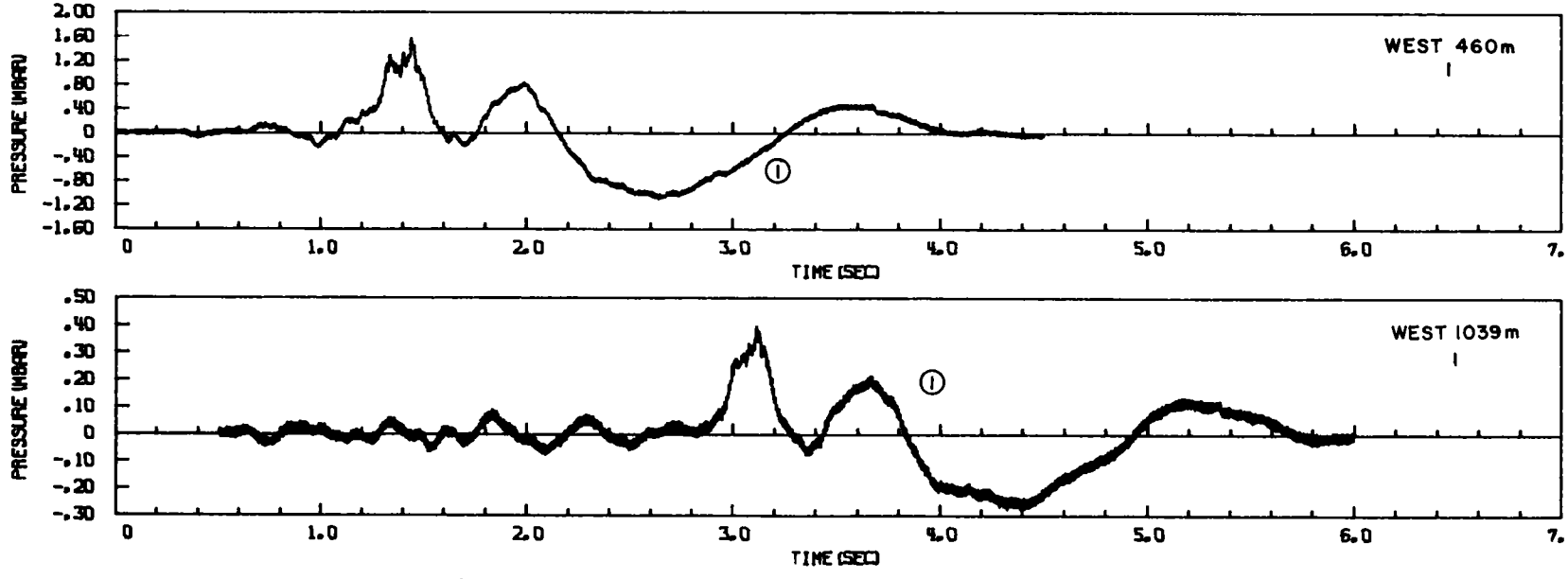

Figure 3.5. Pressure record--W460 and W1039

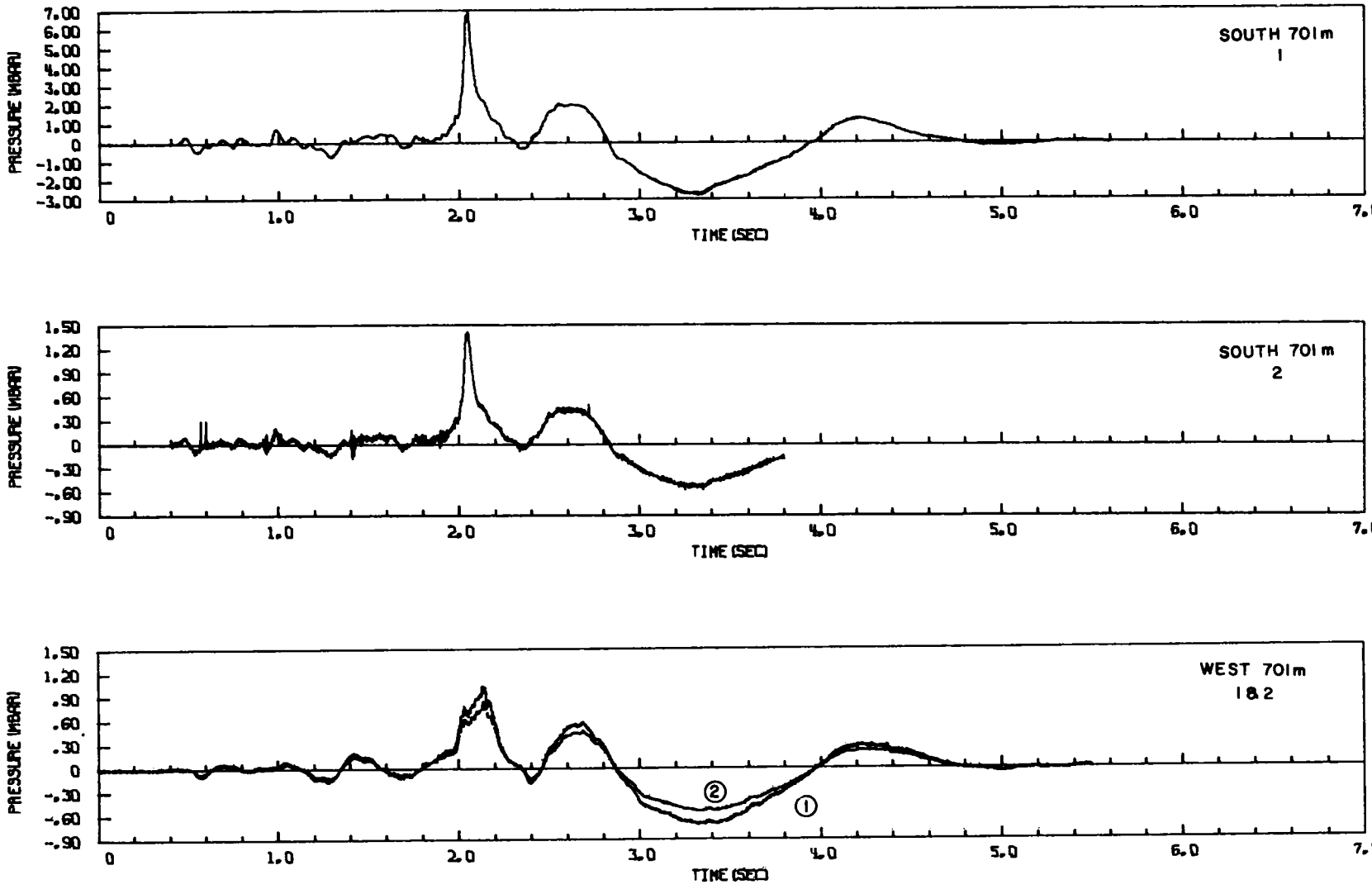

Figure 3.6. Pressure record--S701 and W701

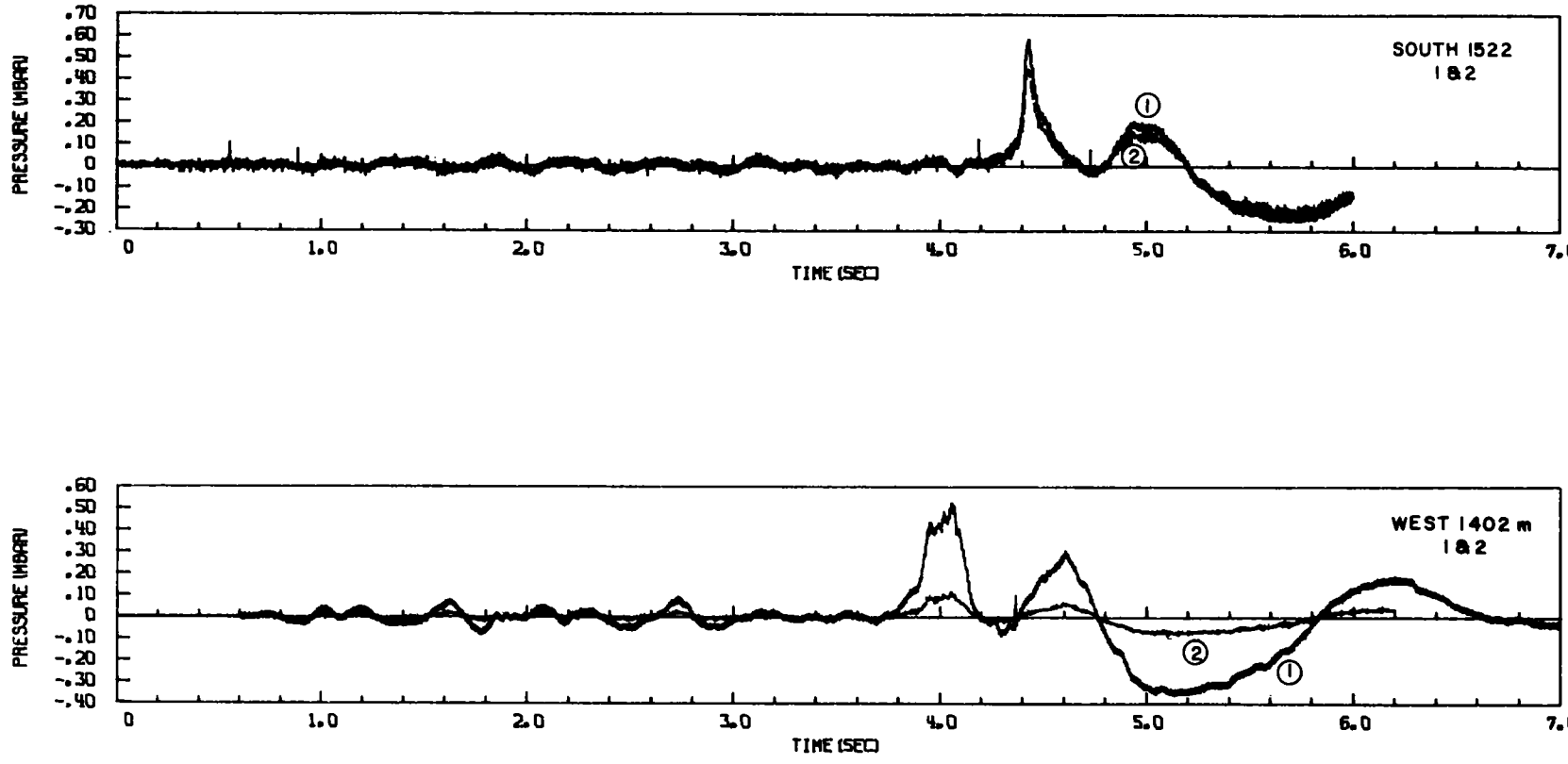

Figure 3.7. Pressure record--S1522 and W1402

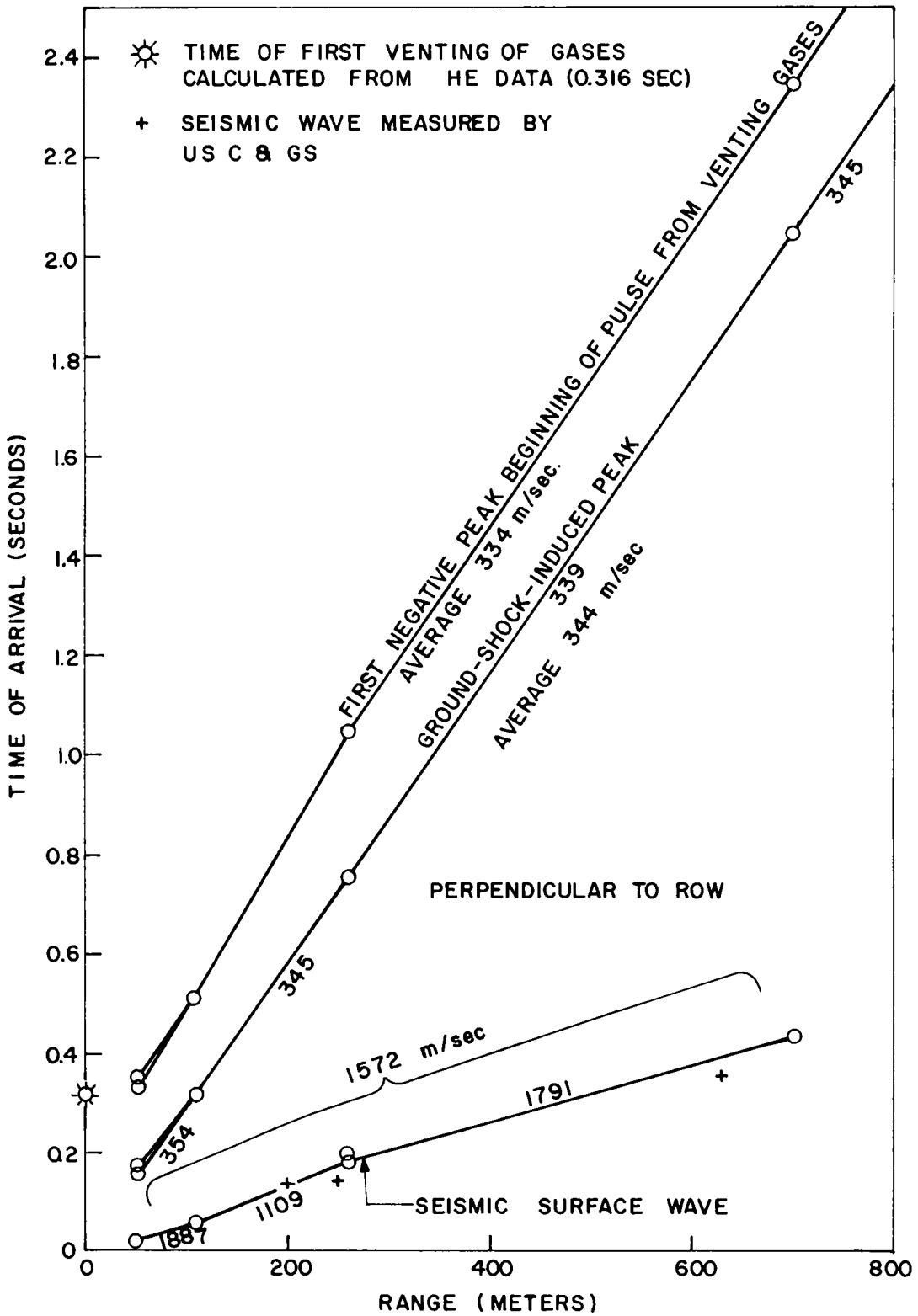

Figure 3.8. Time of arrival data perpendicular to row

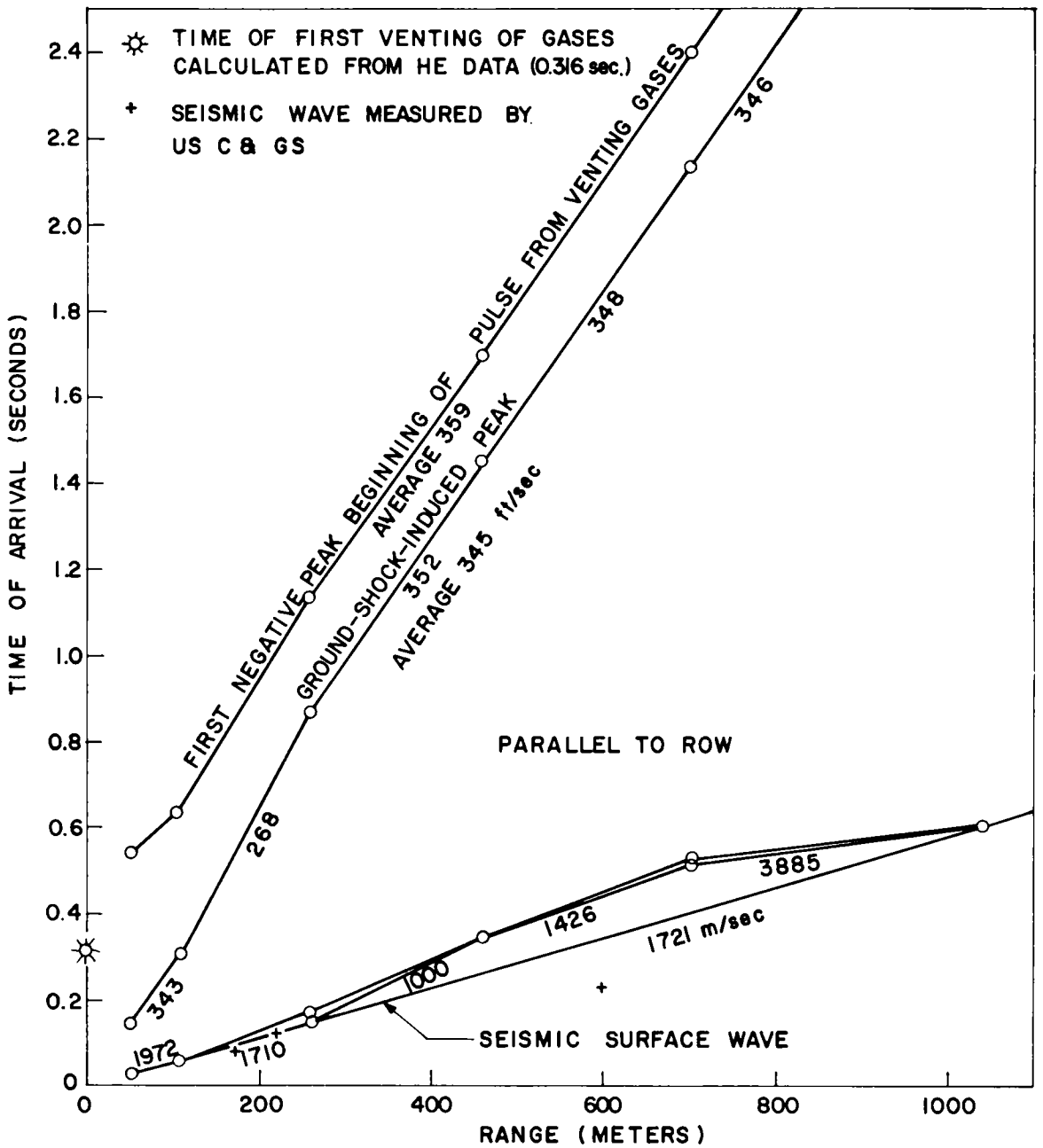

Figure 3.9. Time of arrival data off the end of the row

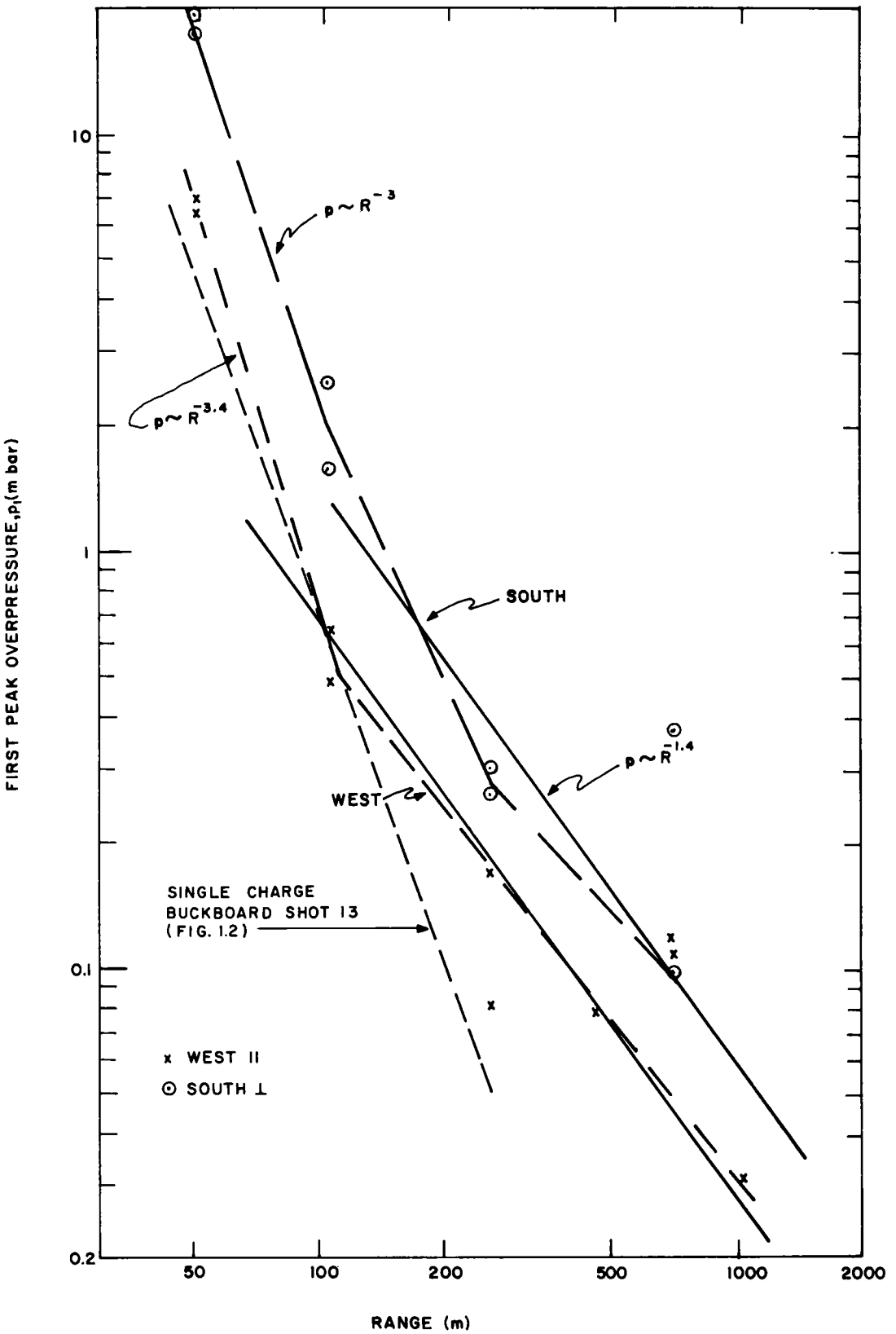

Figure 3.10. First peak overpressure

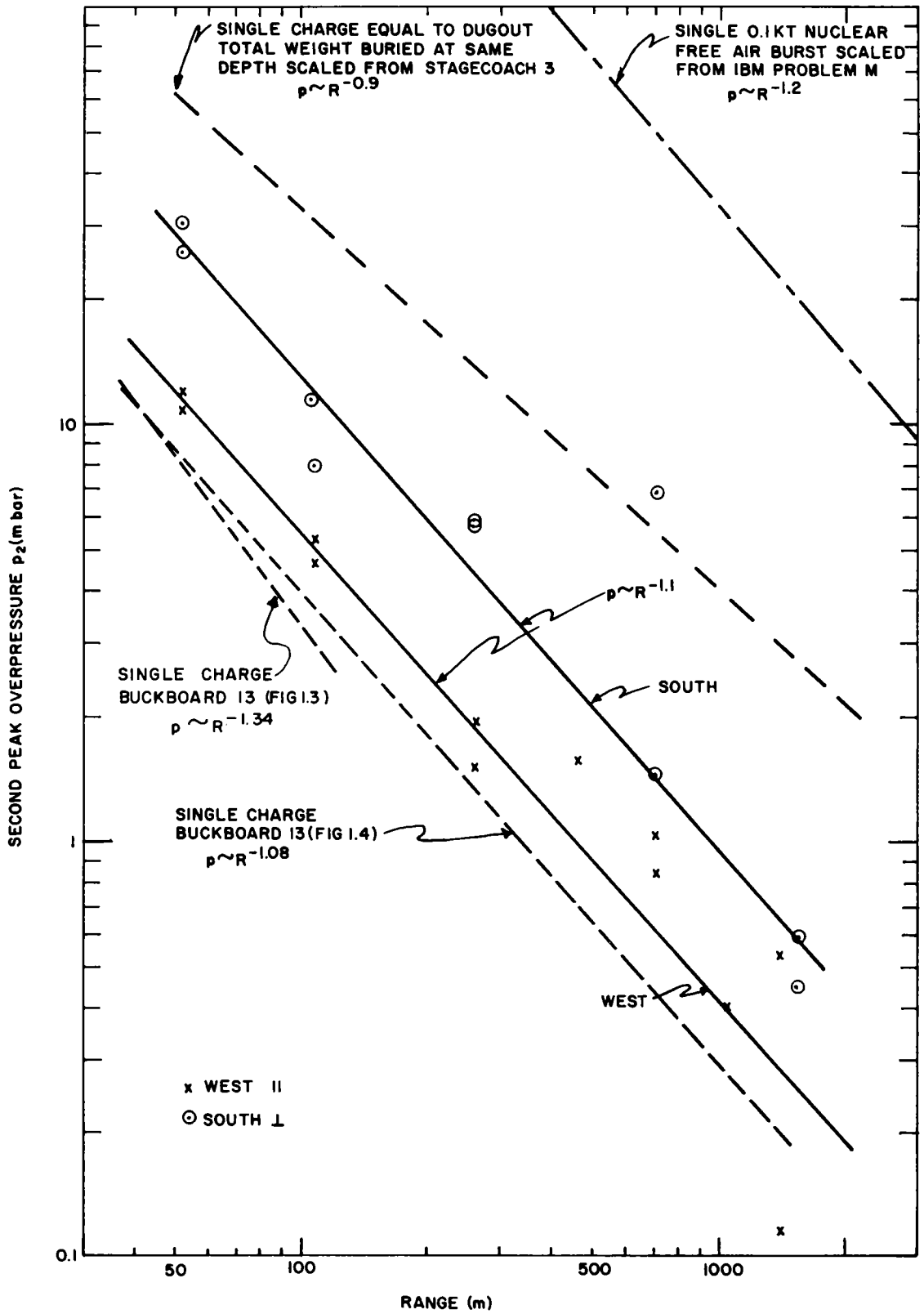

Figure 3.11. Second peak overpressure

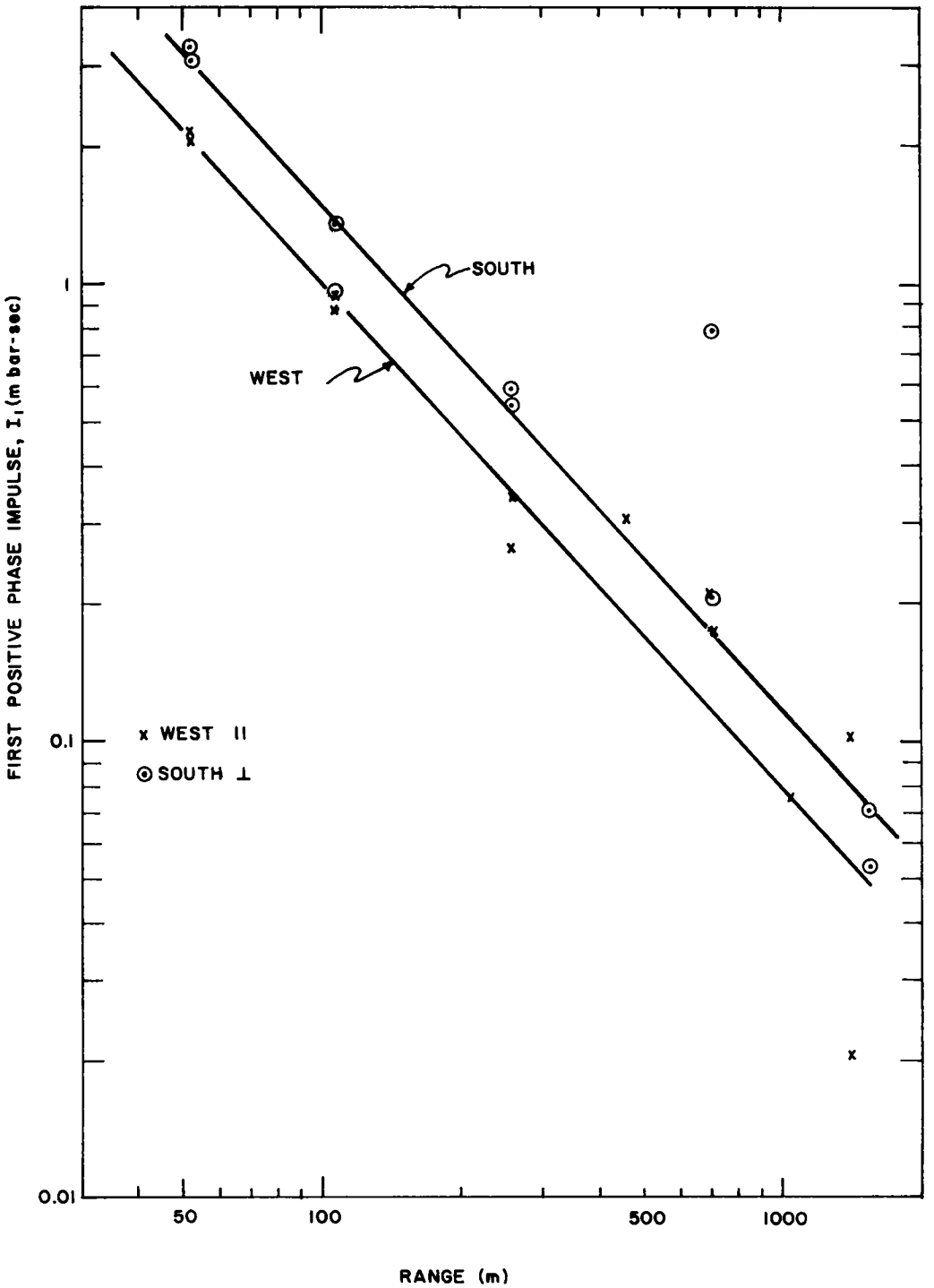

Figure 3.12. First positive phase impulse

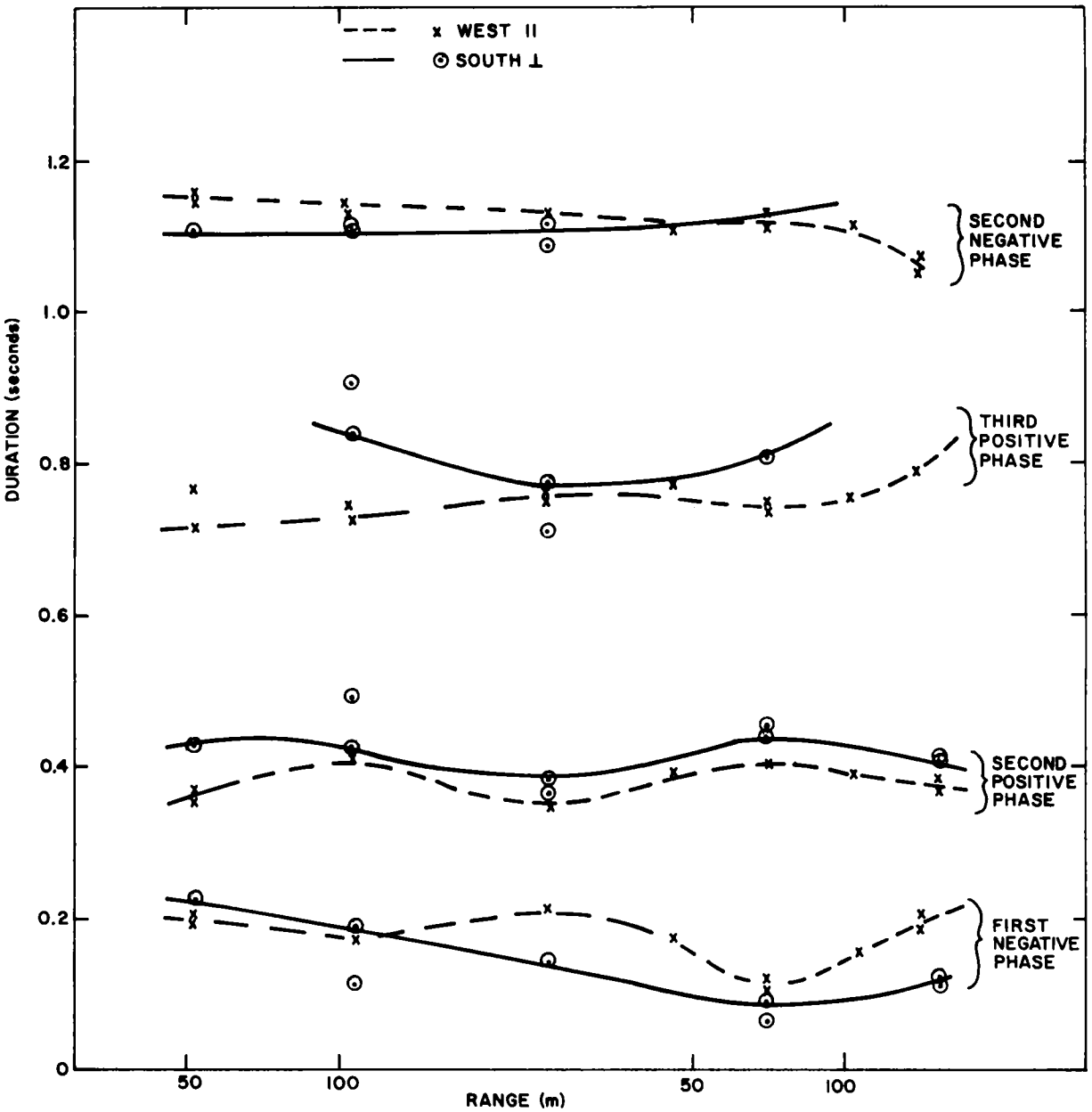

Figure 3.13. Durations of phases after the first

CH 4 - DISCUSSION AND INTERPRETATION

4.1 Introduction

The major components of the Dugout blast wave (Figure 3.1) are the ground-shock-induced pulse* (p_2) and the pulse from venting gases (p_3). Both originate at the epicenter and propagate at essentially sonic velocity in air. The identity of both is established by the fact that their arrival times extrapolated back to the epicenter agree reasonably well with the times of the causative phenomena. The ground-shock-induced peak is dominant at all stations. The peak from venting gases is superimposed on the negative phase following the ground-shock-induced pulse causing an untimely end to that negative phase and apparently enhancing the negative phase following the gas-venting pulse. The positive pressures from venting gases are less than would normally be expected because of the superposition on a negative phase.

A signal preceding the ground-shock-induced pulse travels at a velocity between sonic in air and rock. The wave (p_1) is tentatively identified as a Rayleigh wave. A subsequent experiment has shown that the gage was measuring air pressure induced by the ground motion rather than a signal caused by gage sensitivity to ground motion.

A final positive pulse (p_4) is attributed to a necessary restoration of air to ambient condition.

4.2 Arrival Times and Wave Shape

Few experiments fail to turn up something new or unexpected. In air-blast measurements of Dugout, the succession of positive and negative phases following the initial ones was unexpected.

When a spherically expanding shock wave from a buried explosion strikes the surface, it induces a lens of compressed air over the vicinity of the epicenter. The radius of the expanding sphere is increasing at the speed of sound in the medium. The contact of the expanding sphere with the surface (Curve A, Figure 4.1) is traveling at $Co/\sin\theta$ where Co is sonic velocity and θ is the angle at the center of the detonation between the radius to the contact and the vertical. The strength of the shock attenuates very rapidly ($\sim R^{-2}$). Since its vertical component is responsible for inducing pressure in the air, the vertical component of particle velocity (u) in the soil ($\sim u \cos\theta$) is decreasing even more rapidly with radial distance. Thus, the manifestation of the wave at greater distances decreases rapidly until, as will be shown later, it is not observed at the second gage station on the Dugout event.

---

*The "front porch" of earlier reports.[4,5,6]

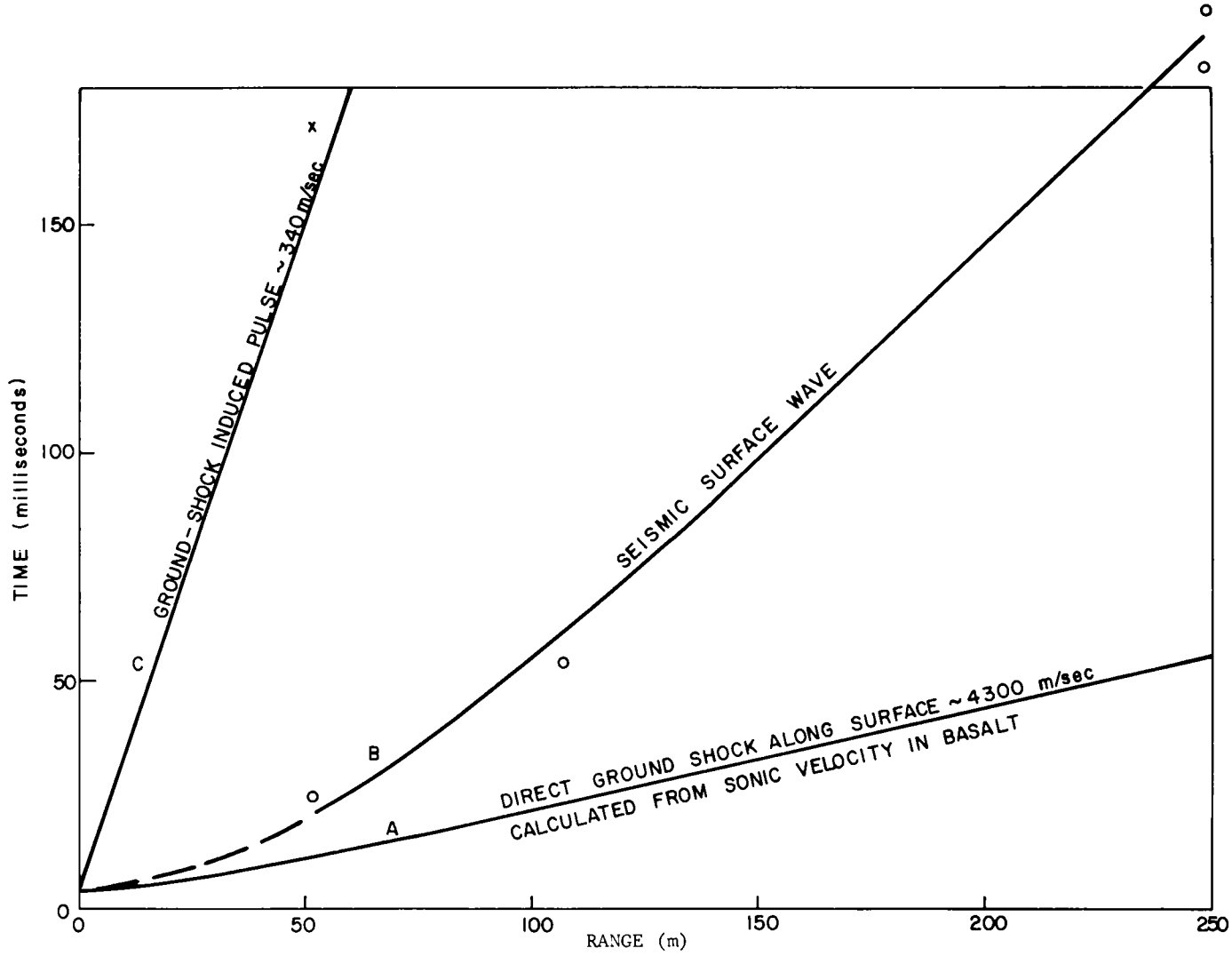

Figure 4.1. Arrival time versus ground range

A ground-shock-induced wave (p_2 in Figure 3.1) generated at the epicenter propagates radially from the epicenter at nearly the sonic velocity in air (Curve C, Figure 4.1).

Between these two waves is a surface seismic wave (p_1, probably a Rayleigh wave, because of the vertical component required to produce an air-pressure pulse) presumably beginning between one or two crater radii and propagating at a velocity between the sonic velocities in rock and air (Curve B, Figure 4.1).

The arrival time data (Figure 4.1) show that the seismic surface wave is the first one observed at the closest station, but, as is pointed out later, the overpressure data suggest some contribution of the direct ground shock at the first gage station.

Arrival times of the seismic surface wave are inconsistent. Perpendicular to the row (south line), they show the wave traveling at an average of 1572 m/sec (Figure 3.8) between 50 and 700 meters. Along the axis of the row (west line), the arrival times are even more erratic but average 1720 m/sec between 50 and 1040 meters (Figure 3.9). These velocities are low for direct propagation in basalt and it is undoubtedly a manifestation of the surface seismic-wave arrival which is being observed. Figures 3.8 and 3.9 show also the arrival of the first ground-motion signal on records of USC&GS stations. Those arrivals suggest a greater propagation velocity than is suggested by the air-pressure measurements. No appreciable delay between seismic-wave arrival and the air pulse it generates would be expected. It is conceivable that in the air-pressure record, there is an earlier signal attributable to the direct ground shock lost in the noise. Even so, neither the overpressure records nor the USC&GS ground-motion records suggest a velocity close to the 4.75 km/sec sonic velocity of the basalt. The arrival times extrapolate to time of arrival of the direct ground shock at the epicenter.

When the spherically expanding shock wave reaches the rock-air interface it (1) is reflected directly downward from the epicenter and (2) imparts to the surface a velocity twice the particle velocity of the shock. The motion of the surface associated with the latter induces a lens-shaped compression in the air immediately above the ground. The velocity of the ground should be equal to the velocity of the air in the ground-shock-induced pulse. In Figure 4.2, the experimentally observed surface velocities associated with measured overpressures are compared with the overpressures associated with equal velocities for a free-air shock wave. Actually the ground-shock-induced blast waves are compression waves rather than shock waves, but the difference in calculated velocities associated with a particular overpressure for shock waves and compression waves is not significant. What is significant is that the overpressures associated with the observed velocities are greater than would be calculated. Why the overpressures are greater is not clear from the data, but it is clear that any attempt to calculate overpressures from surface motion will result in an underestimate of ground-shock-induced peak overpressure.

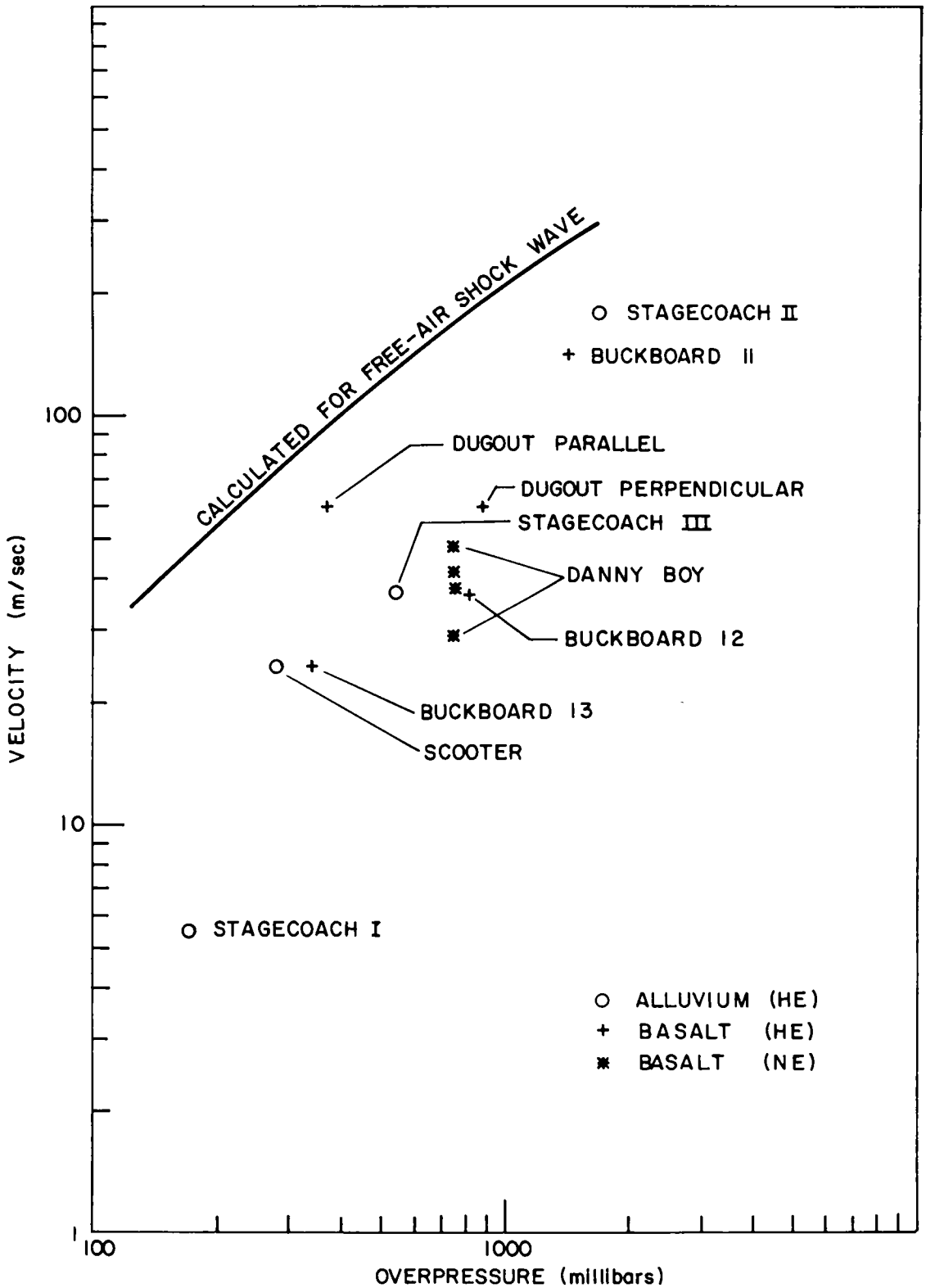

Figure 4.2. Epicenter vertical velocity versus overpressure induced by it

Overpressures at the surface were obtained as follows:

1. Scooter overpressure was obtained from a measured (but not reported) overpressure 0.7 meter above surface zero. It agreed with the extrapolation in Item 2 below at a distance of 3 meters from surface zero.

2. Stagecoach and Buckboard values were obtained from values measured on each event at greater distances extrapolated back to 1 meter from surface zero by assuming overpressure to attenuate as the reciprocal of distance.

3. Danny Boy values were found by extrapolating in the same manner to 1-1/2 meters.

Ingram[11] found the peak surface velocity for Danny Boy to be 29 meters/sec by integration of the record from an accelerometer near surface zero. Carder[12], et al, show initial surface displacement versus time which leads to velocities of about 38 m/sec. Johnson and Higgins[13] report a spall velocity of 41 m/sec. Knox[14] believes the value to be as high as 48 m/sec. The last two values bracket the 45 m/sec found by Nordyke.[15] Nordyke's value for Dugout is also shown in Figure 4.2 with pressures extrapolated to the source from both blast lines. The overpressure values were extrapolated to 1 meter from the epicenter using the attenuation rate $R^{-1.4}$ of Figure 3.10. That for the air blast measured perpendicular agrees well with other experimental results. Were it not for a measured value for Scooter which agreed with linear extrapolations from measured values to the epicenters of other events, one would conclude that a linear extrapolation back to the epicenter was not correct and caused the discrepancy noted earlier between observed and calculated ground-shock-induced overpressures.

At the closest station the seismic pulse and ground-shock-induced pulses are merged. Because of their greatly different propagation velocities they separate at the greater distances. A negative phase follows the ground-shock-induced pulse. Normally the impulse of the negative phase (I_{-1}) is nearly equal to that of the preceding positive phase (I_1). In Dugout, the negative phase is cut short by the superposition of the positive pulse (I_2) from the venting gases. The identity of this pulse is obtained in the following manner. If the time of the negative peak (t_{p-1}) is assumed to be the arrival of the pulse from venting gases and plotted against distance, the intercept at the epicenter is only a bit earlier than the observed time[15] (0.483 seconds) and earlier than the time of first venting of gases calculated from Buckboard data (Figures 3.8 and 3.9).

In the waveforms from Stagecoach, Buckboard, and Scooter, the peak overpressures from the venting gases were dominant. For Dugout, however, they are not because they are superimposed on the negative phase. When peak pressures from venting gases are estimated from a base between the negative phases on either side, those along the west line are about equal to Dugout p_2 along the same line, while those along the south line are about 40 to 50 percent less. A base

between the two negative peaks must be chosen arbitrarily, and considerable scatter therefore results. Another approach is to measure with respect to the negative pressure (p_{-1}) at the time of arrival of the pulse from venting gases (the sum of p_{-1} and p_3). One measure of gas-venting peak so obtained is its relationship to the ground-shock-induced peak: $(p_{-1}+p_3)/p_2$. Values range from 0.36 to 0.48 perpendicular to the row, and from 0.61 to 0.83 off the end of the row. Thus, if gas-venting peaks were not superimposed on a negative phase, they would still be less than 50 percent of ground-shock-induced peaks perpendicular to the row and about 75 percent off the end of the row.

The second negative phase (I_{-2}), being the larger one, is probably enhanced by the presence of the gas-venting pulse. The last positive phase (I_3) is attributed to "overshoot," i.e., to a compensating positive phase required to return the air to ambient conditions.

The overpressures from the seismic wave were, at the closest station, four to five times what they should be to be consistent with the other stations (Figure 3.10). The initial pressure spike at the closest station suggests that perhaps the gage was sufficiently close that it was well within the region in which direct ground shock was directly pulsing the air. However, time-of-arrival data do not support this hypothesis since they were not consistent with the propagation velocities of the direct ground shock. Because of the initial spike, the direct ground shock is greatly attenuated between the first and second stations, and it may well be that there is a transition from direct ground shock to the Rayleigh wave between the first and second gage stations. Between the first two stations, the rates are R^{-3} (south line) and $R^{-3.4}$ (west line). These rates are similar to the $R^{-2.83}$ for similar peaks from Buckboard 13 (Figure A.1). Over much of this same range, on Project Danny Boy, Ingram[11] found the attenuation rate for vertical velocity of the surface to be $R^{-2.1}$. No comparable measurements are available for Dugout. Beyond the second station, the rate ($R^{-1.4}$) agrees with the attenuation rate for ground-shock-induced peaks from single buried charges (Figure A.2, but not Figure A.3) and with the attenuation rate for typical blast waves from surface hemispherical charges. Since the seismic surface wave propagates as a ground wave whereas the ground-shock-induced peak and peaks from surface-burst charges propagate as air waves, the agreement of attenuation rates is probably coincidence.

4.3 Peak Pressures

A recent synthesis[16] of air-pressure data from surface-burst TNT hemispheres has shown that for the pressure region of concern here the pressure attenuation with distance is proportional to $R^{-1.4}$. This agrees with the $R^{-1.34}$ shown in Figure A.2 for the close measurements made on a single charge equal to one of the Dugout charges and buried at the same depth (Project Buckboard Shot 13). When three more distant Buckboard measurements are included, the attenuation rate becomes $R^{-1.08}$ (Figure A.3). Using the more distant gages is subject to possible question because over the range that measurements were made, meteorological effects could alter the rate. It

will be shown later that the Dugout results are in better agreement with the $R^{-1.08}$, however. For a free-air nuclear burst in a homogeneous atmosphere, IBM Problem M suggests an extrapolation below 25 mbar of $R^{-1.22}$. The single charge of Project Buckboard Shot 13 together with IBM Problem M and Danny Boy provide standards against which to compare Dugout results. The peak overpressures of Buckboard Shot 13 are presumed to be those of venting gases although lack of time-of-arrival data prevents a conclusive identification.

The seismic surface wave (p_1) overpressures normal to the row of charges (along the south blast line) are about twice those off the end of the row. At 50 meters the seismic surface-wave peak overpressures along the axis of the row were slightly greater than for a single 18,000-kg charge (from Figure A.1), while perpendicular to the row they were more than three times the single charge values. Beyond 100 meters, the difference in attenuation rates makes the row-charge pressures many times those of the single charge.

The ground-shock-induced overpressures (p_2) (Figure 3.11) are attenuated along the south line at about $R^{-1.12}$. Figure 3.11 shows the same rate of attenuation applied also to data from the west blast line. The blast wave along the west line was different, however, in that at the two closest stations the dominant peak occurred early in the ground-shock-induced pulse, while at the more distant stations, a later peak was dominant. (Compare the records for the west line in Figures 3.3 through 3.6.) The effect is illustrated in Figure 4.3. Note that in Figure 3.11 the values at 460 and 701 meters and one value at 1402 meters were considered too high, but credence was given to the value at 1039 meters. In contrast, in Figure 4.3 which considers only the later second peaks, emphasis is given the larger value at 1402 meters, disregarding that at 1039 meters. This distinction between the two ground-shock-induced peaks along the west line is supported by their time of occurrence as discussed below. However, the low-attenuation rate indicated in Figure 4.3 for the later ground-shock-induced peak ($p \sim R^{-0.77}$) is incredible because:

1. It does not agree with the rate for the south blast line.

2. The rate is much too low when compared with that for single charges. Single charges would imply either $p \sim R^{-1.4}$ or $p \sim R^{-1.2}$, but the data in no way support so high an attenuation.

The ground-shock-induced peak overpressure (p_2) is always larger than the peak from the seismic wave peak (p_1) but by varying amounts because of the difference in attenuation rates. For example, ground-shock-induced peaks are twice the seismic peaks at 50 meters and 10 times the seismic peaks at 500 meters.

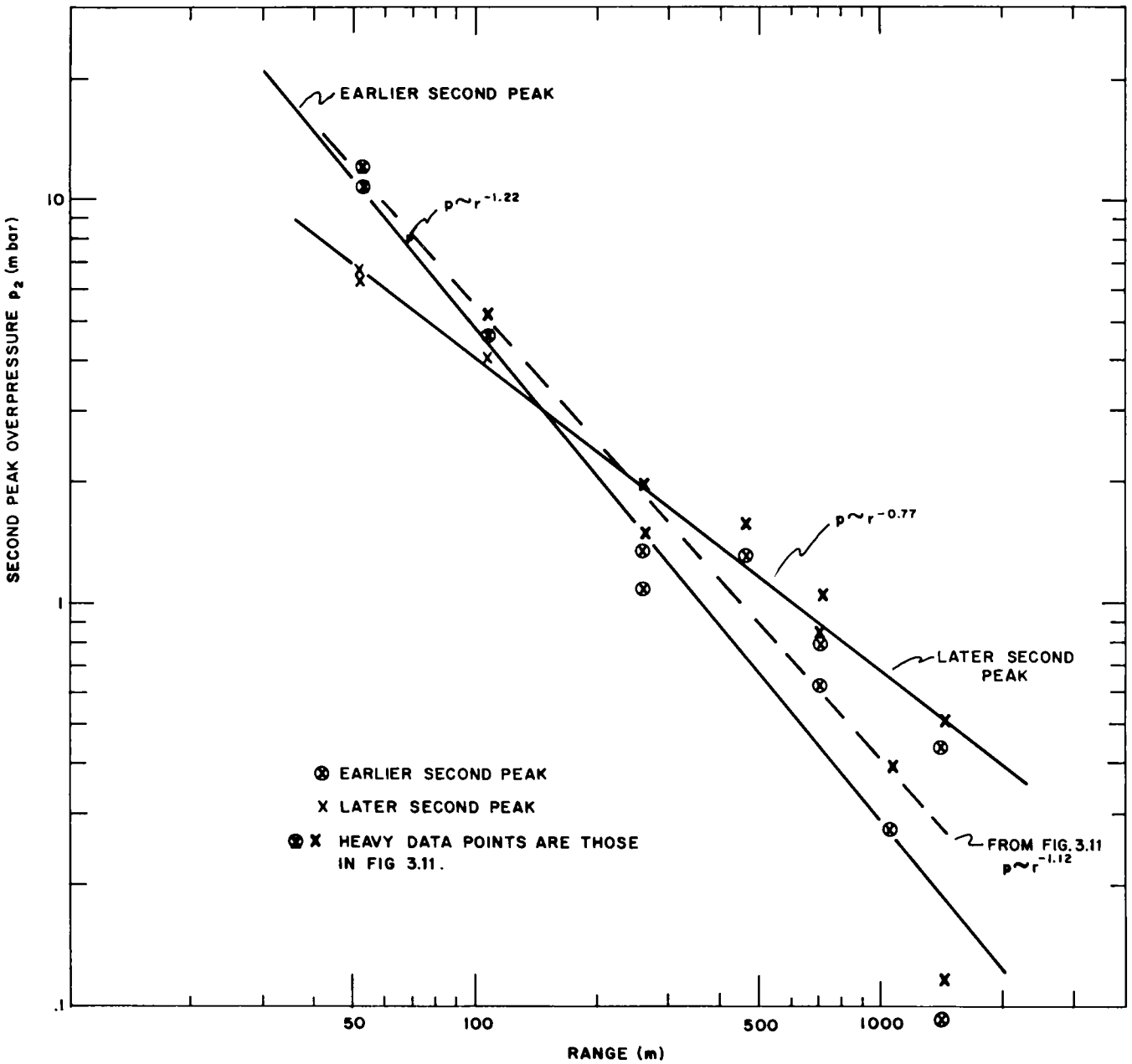

Figure 4.3. Second peak overpressure versus range

Peak overpressures perpendicular to the row, as shown in Figure 3.11, are slightly more than twice those along the axis of the row.

Because of different attenuation rates between single- and row-charge data, the relationship of blast from the row charge to blast from single charges, equal to one of the charges in the row, varies with range. The following results are obtained using Figure 3.11 and the close-in data of Figure A.2:

Range (m)	Ratio to Single Charge: Perpendicular (south)	Ratio to Single Charge: Parallel (west)
50	3.35	1.45
100	4.00	1.25
250	4.87	2.05
500*	5.70	2.45
1000*	6.35	2.75

*Based on extrapolation of single-charge data.

When both the close data and the distant (microbarograph) data are used from Figure A.3, the attenuation rates are more nearly constant with range and the comparison shows the following:

	Range (m)	Ratio to Single Charge: Perpendicular (south)	Ratio to Single Charge: Parallel (west)
(a)	50 to 1000	3.28	1.39

Using the 11-charge experiment described in Chapter 1[7] as a standard gave:

	Ratio to Single Charge: Perpendicular (south)	Ratio to Single Charge: Parallel (west)
(b)	5.25	1.80

For the 5-charge Dugout row, comparison (a) above suggests a 10-percent increase over the single-charge peak overpressure per additional charge off the end of the row and a 57-percent increase perpendicular to the row. For the small 11-charge experiment, the values are 8 and 43 percent, respectively. These two experiments suggest a decreasing contribution per additional charge as the number of charges in the row is increased.

A simple way of expressing this result is shown in Figure 4.4. The ratio of peak overpressure from multiple charges to that of a single charge can be expressed as a function of the number of charges.

Perpendicular to the row:

$$\frac{P_{row}}{P_{single}} = n^{0.7} \quad .$$

Off the end of the row:

$$\frac{P_{row}}{P_{single}} = n^{1/4} \quad .$$

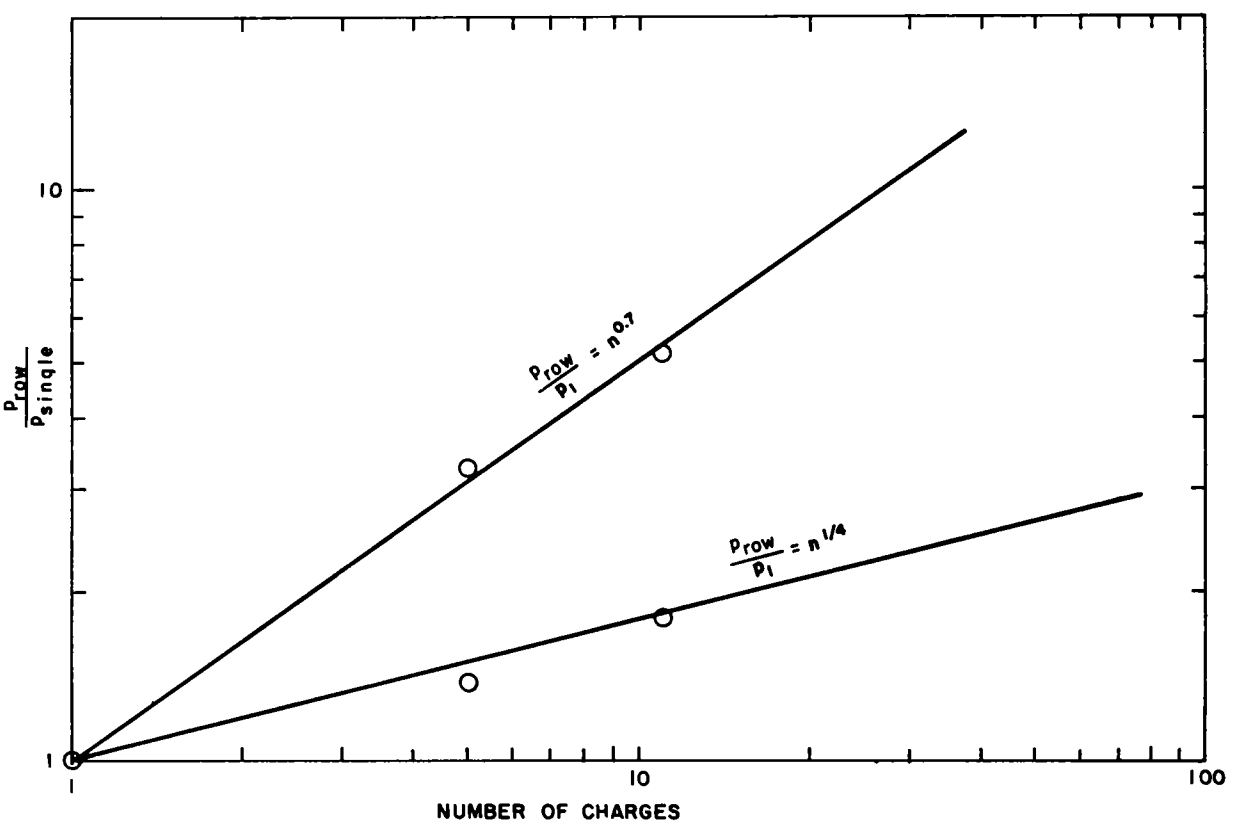

Figure 4.4. Ratio of row- and single-charge pressures versus number of charges

Peaks from the Dugout 5-charge explosion were those of the ground-shock-induced pulse while the peaks from the 11-charge shot may have come from venting gases. Thus, they may not be directly comparable, and the agreement which permitted the above relationships may be coincidence.

In making the above comparison, the values from a least-square fit to the Buckboard Shot 13 data (Figures A.2 and A.3) were compared with data from Figure 3.11. No attempt at a least-square fit was made for Figure 3.11 or other figures in Chapter 3, since to do so incorrectly assumes all data are equally credible. Instead, eyeball fits have generally accorded more credence to data from closer stations.

The first negative peak pressure (p_{-1}) (Figure A.6) is attenuated at about the same rate as the second positive peak overpressure ($p \sim R^{-1.1}$). There is no clearly defined difference along the two blast lines.

The third positive peak overpressure (p_3) (Figure A.7) is attenuated at the same rate as the second positive peak ($p_2 \sim R^{-1.12}$). The peak values normal to the row are twice those off the end.

It is this third positive overpressure wave (p_3) which has, on the basis of time-of-arrival data (Figures 3.8 and 3.9), been identified as the pulse from venting gases superimposed on the first negative phase. The time of arrival was taken as the time of the negative peak of the preceding negative phase, which is not a precise measure of arrival time of the pulse from venting gases. Because of the superposition on the first negative phase, the peak positive pressures of this wave are less than those of the ground-shock-induced wave. The wave from venting gases is no longer the dominant peak as in the case of the typical wave from Scooter (Figure 1.1). In the expressions developed above, the data from the 5-charge row (Dugout) are the ground-shock-induced peaks whereas those from the 11-charge row are from the gas-venting peaks. This may be because of the slightly deeper cube-root scaled depth of burial of the Dugout charges or it could be due to a soil-rock difference. The expressions developed above should be modified when data become available for equal scaled burial depths in identical media.

The second negative peak pressure (p_{-2}) (Figure A.8) off the end of the row also decreases with distance as $R^{-1.1}$. However, the scatter in the results normal to the row precludes a well-defined attenuation rate. Peaks normal to the row are 50 percent higher than those off the end.

The fourth positive peak overpressure (p_4) (Figure A.9) is attenuated off the end of the row at a slightly lower rate than for the other cases ($p \sim R^{-1.05}$). The rate normal to the row, as defined by the first three stations, is about the same. Here again, peak pressures perpendicular to the row are about twice those parallel to it.

All of the peaks fall off with distance at about the same rate ($p \sim R^{-1.1}$) and at a rate comparable to that for single charges $p \sim R^{-1.08}$ (Figure A.3).

The west blast line passed over a low ridge and down a shallow grade (Figure 4.5). Terrain effects on blast waves from above surface bursts have been observed on earlier experiments. Measurements were made at pressure levels from 7.0 to 70 mbars over ridges five times as high as that on Dugout,[17] from 5 to 160 mbars over the same ridge,[18] and from 500 mbars to 4 bars on a similar ridge.[19] In addition, scale model experiments had been performed on idealized ridges.[20]

The results of these experiments show that peak overpressures are larger on the inclining face of the ridge and smaller on the declining face than on a level surface. At the top of the ridge, the peak overpressures are essentially the same as for a level surface in the idealized case, but in practice may remain high until just behind the top of the ridge. Impulse data are not as plentiful, but they indicate the same trends.

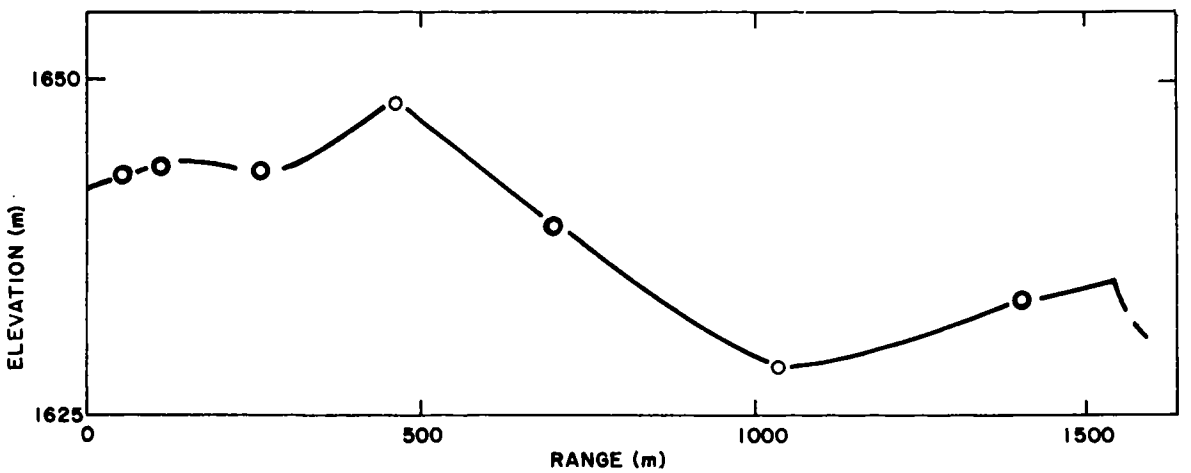

Figure 4.5. Profile of west blast line

The model experiment with an idealized ridge shows that the increase in peak overpressure over that of a level plane on the forward slope and the decrease on the rearward is related to the steepness of the slope. For a single relatively low burst height and at a constant distance from the charge, the increase or decrease over level plane values was found to be as follows:

Slope Angle (deg)	Increase on Forward Slope (%)	Decrease on Rearward Slope (%)
30	100	50
17.1	50	25
5.7	20	5 - 10

Since the average slope along the west blast line was only about 2-1/2 degrees (Figure 4.5), the effect of terrain must have been small indeed--probably departing less than +10, -5 percent of level terrain values.

Turning to the values for the maximum (second) positive peak (Figure 3.11) from the top of the ridge (460 m west), the value is not 10 percent but 50 percent greater than indicated by the fit shown to the other data. At the next station (701 m west), the

values for two gages on the downward slope averages 55 percent greater rather than a few percent less as would be indicated by the model experiment. The reader is reminded of the difficulty of calibrating gages in this range. This fact alone leads to the postulate that the departures because of terrain effects are lost in those because of inaccuracies of gage calibration.

Earlier air blast from row charges was compared with that from a single charge equal to one of the charges in the row. The air blast can also be compared with that from a single charge of the combined weight of the five (90,000 kg) at the same actual depth (17.9 meters). Accordingly, the charge is at a shallower scaled burial depth, one which corresponds most closely to that of Stagecoach III. In Stagecoach III, the peak from venting gases is the dominant one and the ground-shock-induced peak is of lesser consequence. The comparison shows that at a typical scaled range, ground-shock-induced peaks from Dugout perpendicular to the row are only one-third the gas-venting peaks to be expected from the larger charge. Dugout peaks off the end of the row are only one-fifth the gas-venting peaks from a 90,000-kg charge at 17.9 meters. Such a comparison is not especially meaningful except to show that spreading out the charge in a row does reduce the air blast.

4.4 Impulse

The first positive-phase impulse (Figure 3.12) is attenuated with distance along both blast lines at nearly the same ratio as peak pressures ($I_1 \sim R^{-1.1}$). The impulse normal to the row is about 50 percent greater than that off the end of the row.

The first negative-phase impulse (Figure A.10) has too much inherent scatter to permit determination of either rates of falloff or differences between the two blast lines.

The second positive-phase impulse (Figure A.11) is also attenuated at the rate of $R^{-1.1}$ normal to the row, but no value has been obtained for the parallel line because of scatter.

The second negative-phase impulse (Figure A.12) was the largest of all pulses. Off the end of the row the rate of falloff was again $R^{-1.1}$. No value was obtained for the blast line normal to the row because of scatter in the data.

The third positive-phase impulse (Figure A.13) was less well defined than the other pulses, but along the blast line off the end of the row the rate of attenuation was R^{-1}.

4.5 Durations

Presumably because of the differences in the propagation rate of the seismic surface wave and the ground-shock-induced wave, the duration of the first positive phase (which includes both waves) increases with an increase in ground range. When scaled by the cube root of the total charge weight, the Dugout first positive-phase durations agree with those for Buckboard 13. After the end of the first positive phase, subsequent events occur later along the west

line than along the south line. The second peak and the end of the first positive phase occur later along the west line. The difference is attributable to the transit time along the length of the row.

Earlier it was noted that along the west line the dominant peak overpressure shifted from an earlier peak to a later one. This is evidenced by considering the time interval between the dominant peak and the end of the first positive phase. When the proper identity of peaks is retained, the times for each of the peaks is as shown in Figure 4.6.

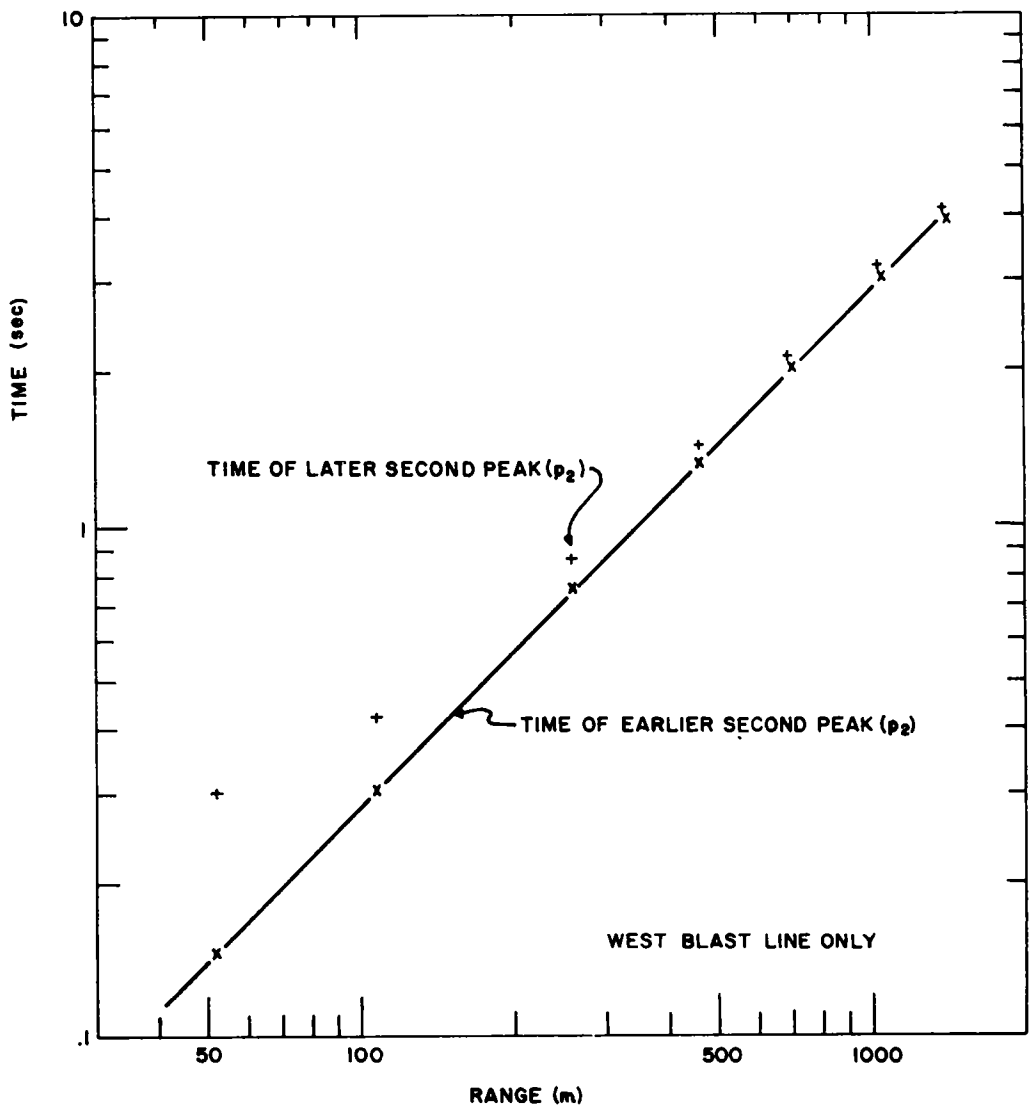

Figure 4.6. Comparison of times of earlier and later second peaks

4.6 Implications

Two to four millibars is the threshold for breaking plate-glass windows. This value occurs from a single charge equal to one of the charges in the Dugout row at a distance of 145 meters. Buckboard, Scooter, and Stagecoach experiments showed no appreciable difference in peak overpressure because of the different media, implying that pressures from an HE row charge in alluvium would be about the same as those measured on Dugout. Sedan gave peak overpressures four times those expected from a comparable HE detonation, and Danny Boy gave pressures about one-third the expected values. Thus, a single-charge nuclear explosion equal in yield to one of the HE charges in Dugout might pessimistically have broken windows to a range of 400 meters. The results of Dugout show that such damage would occur to 1.8 km perpendicular to a row of five such nuclear charges and to 0.8 km from the nearest charge along the axis of the row. These distances are equivalent to a range of 65 and 30 km, respectively, for a row of five 1-megaton nuclear explosions, or 140 and 65 km for a row of five 10-megaton nuclear explosions, even if no atmospheric ducting or refraction occurred to carry the pressures farther.

4.7 Data Adjustments

It was observed earlier and is obvious from Figures 3.2 to 3.7 that certain of the records exhibited systematic departures from an arbitrary standard. The standard used was the fit to the data shown in Figures 3.10 to 3.13 and A.6 to A.13. Occasional departures from those fits would suggest that the fits had been poorly selected. If, however, the departures were a uniform percentage for both positive and negative values, a systematic deviation is indicated.

Eight records gave an indication of systematic deviation as suggested by Table 4.1, which shows the ratio of the measured value to the value obtained by the fit to the other data. Figures 4.7 to 4.12 show the records of Figures 3.2 to 3.7 after those listed in Table 4.1 have been adjusted by the average values listed in the table. As a result of the adjustment, the values of Table 3.1 become those shown in Table 4.2.

These adjustments cause the later second peak values which had appeared to be attenuated at $p \sim R^{-0.77}$ (Figure 4.2) to agree more closely with the attenuation rate shown in Figure 3.11 ($p \sim R^{-1.1}$) at ranges greater than 150 meters.

The agreement of records from gages at identical locations, evidenced by Figures 4.7 to 4.12 after these adjustments have been made, are ample evidence that the observed lack of agreement noted in Figures 3.2 to 3.7 is a systematic one. This tends to confirm that the departures were due to calibration errors. It does not assure that the adjustments made were the best ones.

TABLE 4.1

Ratio of Value Recorded to Value from Fitting

Gage	Second Positive Peak p_2	Third Positive Peak p_3	Fourth Positive Peak p_4	Second Negative Peak	First Positive Phase Impulse I_1	Second Positive Phase Impulse I_2	Third Positive Phase Impulse I_3	Second Negative Phase Impulse I_{-2}	Average*
S107-1	0.67	0.67	0.67	0.62	0.69	0.69			0.67
S701-1	4.90	4.18	3.54*	4.67	4.62	4.74			4.62
S1522-2	0.76	0.81			0.75	0.74			0.76
W259-2	0.81	0.92	0.85	0.87	0.75	0.68	0.92		0.83
W460-1	1.58	2.13	1.54	1.75	1.67		1.74	1.65	1.72
W701-1	1.78	2.37	1.50	1.83	1.79		1.56	1.77	1.80
W701-2	1.41	1.92	1.15	1.40	1.45		1.23	1.38	1.42
W1402-1	1.88	3.08*	1.94	2.14	2.06		2.07	1.89	2.00
W1402-2	0.41	0.68*	0.45	0.49	0.414			0.41	0.43

*Underlined values were not used in obtaining averages.

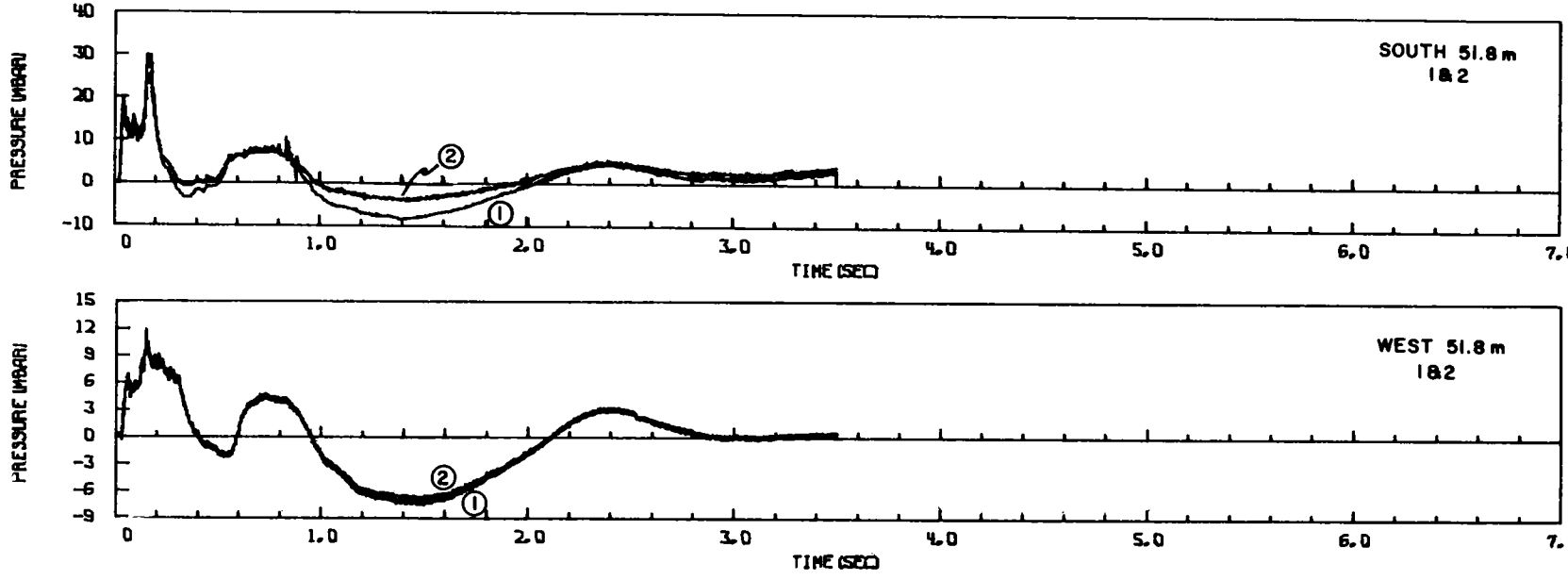

Figure 4.7. Adjusted pressure record--S51.8 and W51.8

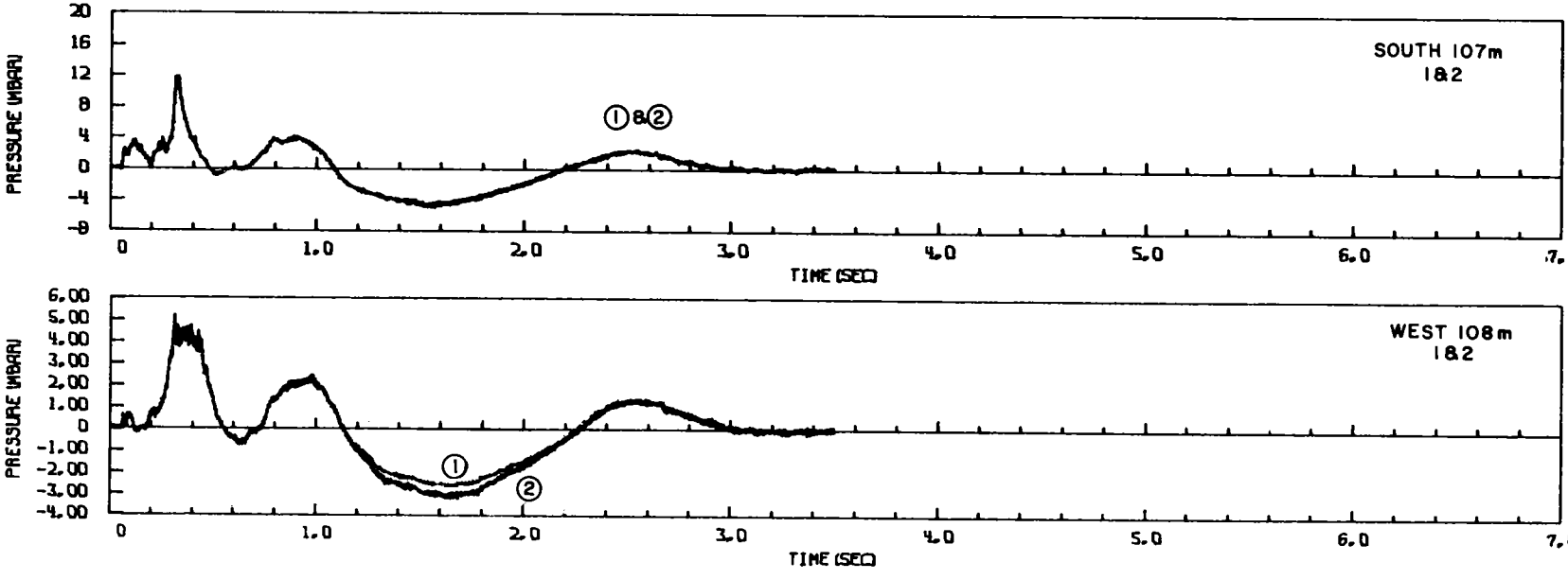

Figure 4.8. Adjusted pressure record--S107 and W108

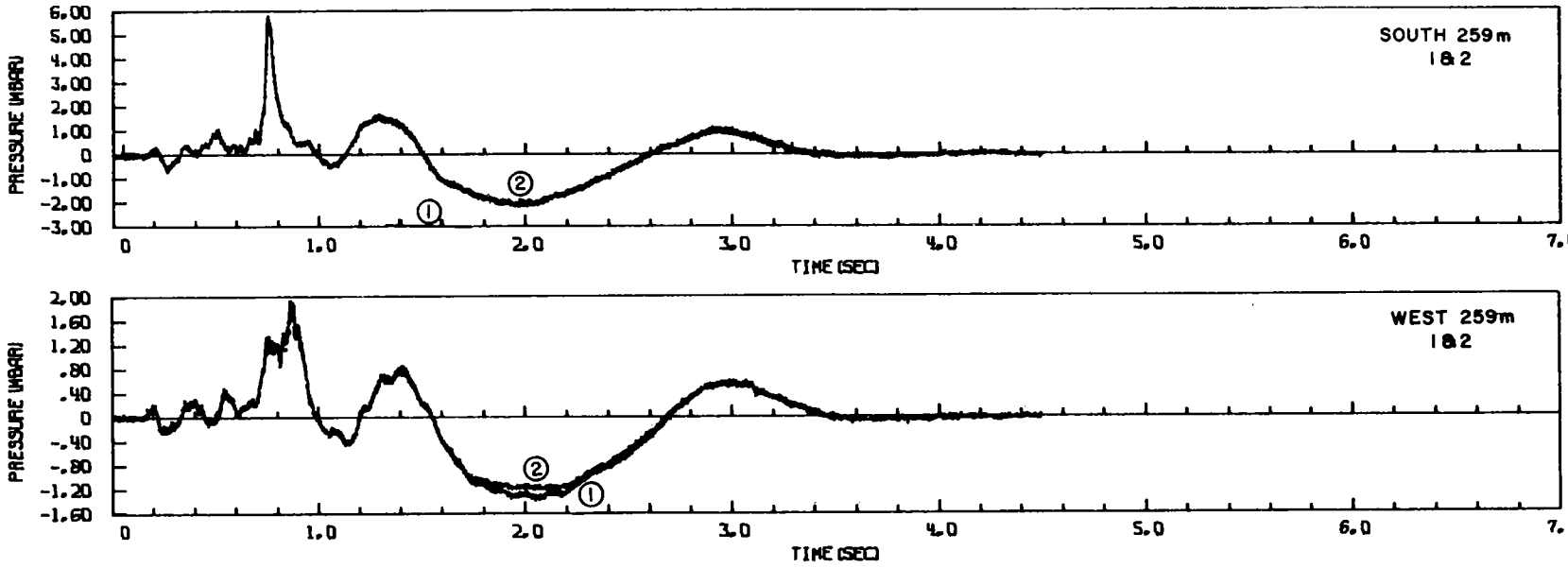

Figure 4.9. Adjusted pressure record--S259 and W259

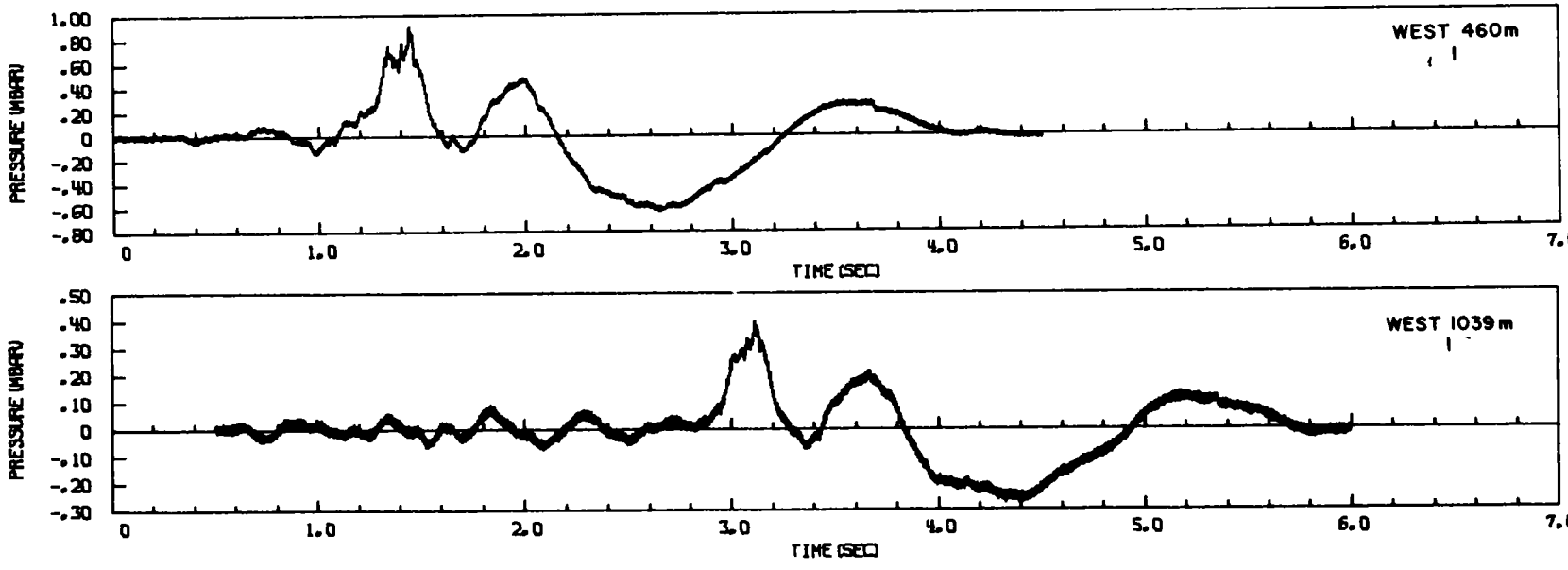

Figure 4.10. Adjusted pressure record--W460 and W1039

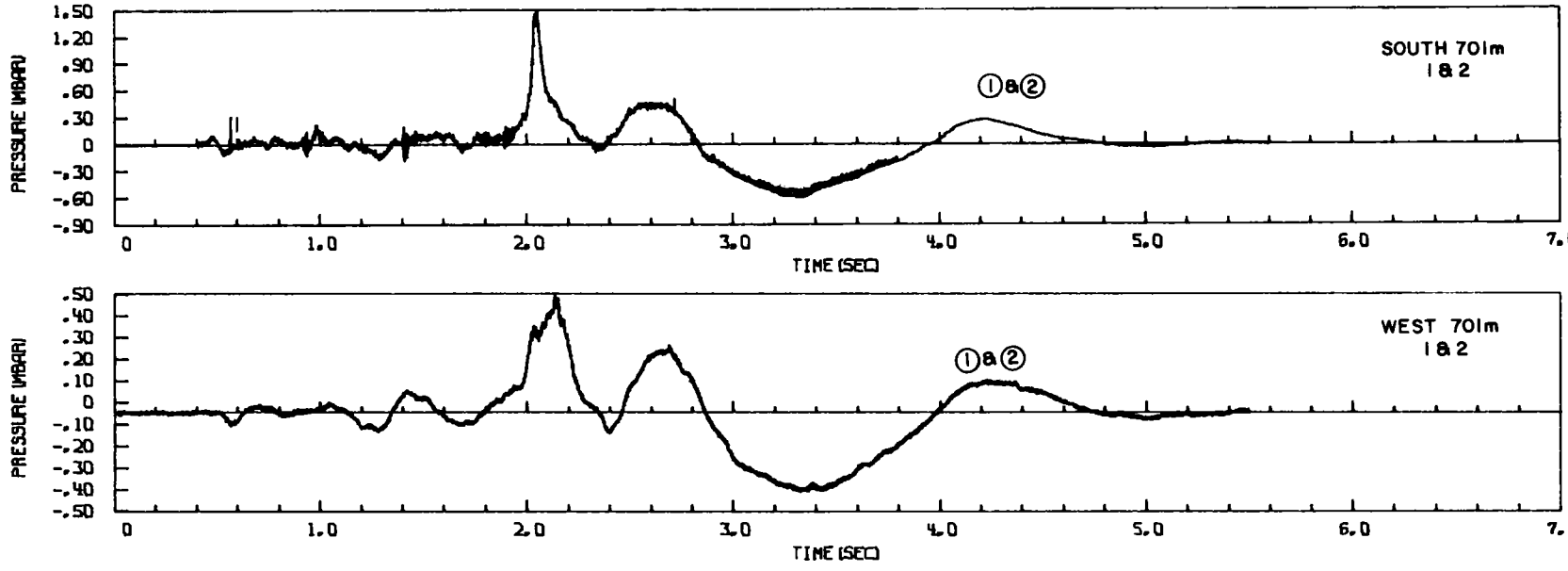

Figure 4.11. Adjusted pressure record--S701 and W701

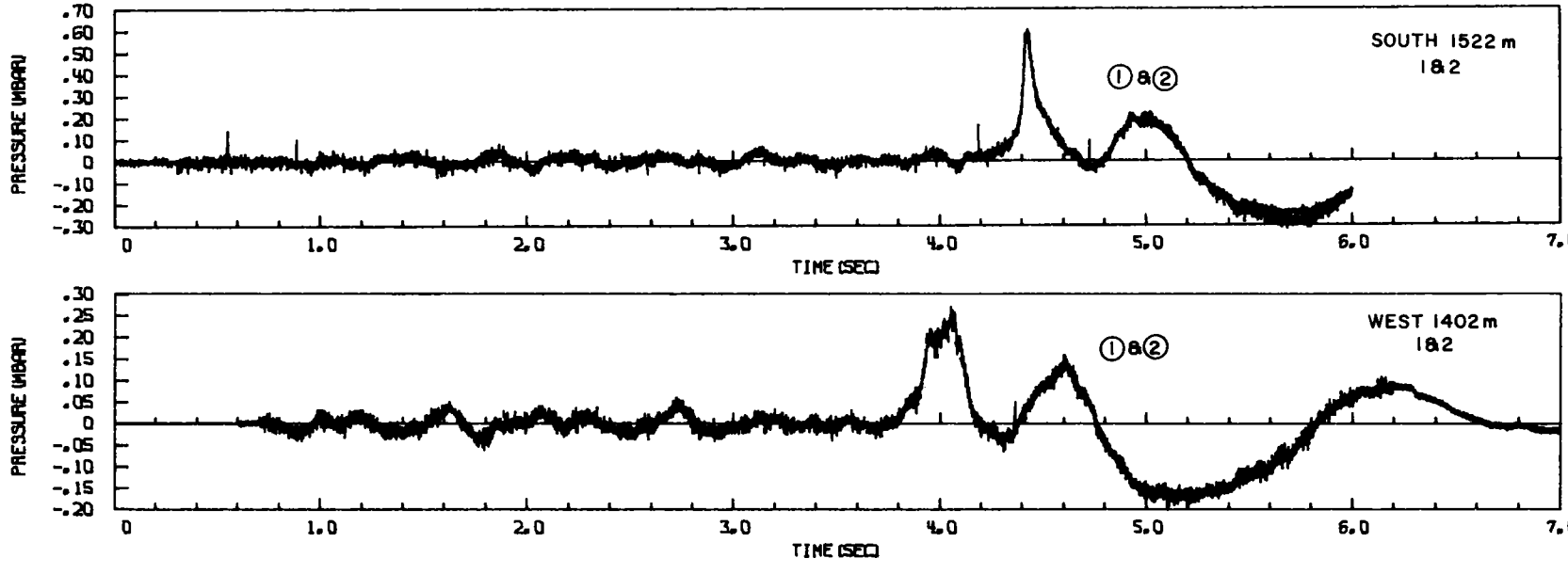

Figure 4.12. Adjusted pressure record--S1522 and W1402

TABLE 4.2

Adjusted Pressure Measurements

Gage	t_a (sec)	p_1 (mbar)	t_{p_1} (sec)	p_2 (mbar)	t_{p_2} (sec)	I_1 (mbar-sec)	t_{I_1} (sec)	p_{-1} (mbar)	$t_{p_{-1}}$ (sec)	I_{-1} (mbar-sec)	$t_{I_{-1}}$ (sec)
S51.8-1	0.0245	19.41	0.041	30.26	0.157	3.29	0.287	-3.86	0.335	0.441	0.509
-2	0.0245	17.30	0.038	25.82	0.172	3.04	0.308	-1.25	0.353	0.0469	0.385
S107-1	0.0535	2.37	0.062	11.93	0.313	1.43	0.471	-1.045	0.507	0.0454	0.657
-2	0.054	2.54	0.065	11.52	0.313	1.36	0.477	-0.975	0.515	0.0566	0.590
S259-1	0.197	0.261	0.208	5.72	0.754	0.544	0.991	-0.599	1.047	0.0483	1.132
-2	0.1845	0.303	0.204	5.77	0.753	0.589	0.989	-0.543	1.047	0.0386	1.130
S701-1	0.439	0.081	0.478	1.50	2.049	0.170	2.306	-0.087	2.342	0.00403	2.390
-2	0.436	0.097	0.471	1.42	2.048	0.208	2.317	-0.057	2.352	0.00207	2.380
S1522-1				0.589	4.430	0.0704	4.686	-0.048	4.740	0.00276	4.797
-2	4.119*			0.593	4.432	0.0707	4.677	-0.063	4.760	0.00272	4.797
W51.8-1	0.0295	7.03	0.056	12.00	0.145	2.15	0.392	-2.45	0.546	0.277	0.593
-2	0.0275	6.48	0.055	10.77	0.145	2.04	0.398	-2.19	0.535	0.243	0.590
W108-1	0.0565	0.493	0.064	5.25	0.310	0.952	0.547	-0.702	0.621	0.0635	0.723
-2	0.0575	0.651	0.061	4.62	0.308	0.876	0.550	-0.861	0.623	0.0697	0.725
W259-1	0.169	0.08	0.174	1.95	0.865	0.342	0.987	-0.482	1.131	0.0580	1.205
-2	0.145	0.205	0.204	1.81	0.878	0.318	0.983	-0.445	1.135	0.0541	1.201
W460-1	0.345	0.046	0.365	0.91	1.442	0.180	1.589	-0.135	1.696	0.0104	1.763
W701-1	0.514	0.066	0.580	0.578	2.135	0.118	2.343	-0.114	2.398	0.0069	2.463
-2	~0.529	0.077	0.567	0.594	2.136	0.122	2.345	-0.108	2.402	0.0112	2.458
W1039-1	0.601	0.031	0.622	0.398	3.113	0.0759	3.279	-0.079	3.361	0.00759	3.436
W1402-1				0.264	4.057	0.052	4.196	-0.046	4.297	0.0035	4.382
-2				0.270	4.053	0.048	4.172	-0.065	4.309	0.0032	4.382

*Arrival of second pulse. First wave not discernible.

TABLE 4.2 (cont)

Gage	p_3 (mbar)	t_{p_3} (sec)	I_2 (mbar-sec)	t_{I_2} (sec)	p_{-2} (mbar)	$t_{p_{-2}}$ (sec)	I_{-2} (mbar-sec)	$t_{I_{-2}}$ (sec)	p_4 (mbar)	t_{p_4} (sec)	I_3 (mbar-sec)	t_{I_3} (sec)
S51.8-1	10.70	0.837	2.43	0.938	-8.99	1.379	5.86	2.039	4.91	2.390		
-2	8.90	0.800	2.61	0.966	-4.44	1.433	2.43	1.904	5.52	2.392		
S107-1	4.21	0.892	1.09	1.082	-4.66	1.569	3.22	2.191	2.61	2.527	1.02	~3.030
-2	4.13	0.908	1.05	1.081	-5.04	1.515	3.40	2.184	2.58	2.491	1.07	~3.089
S259-1	1.58	1.301	0.364	1.497	-2.24	1.957	1.53	2.613	1.02	2.932	0.375	3.322
-2	1.67	1.295	0.393	1.505	-2.16	1.984	1.44	2.588	1.10	2.905	0.453	3.359
S701-1	0.446	2.553	0.131	2.826	-0.606	3.323	0.40	3.957	0.28	4.228	0.108	4.765
-2	0.456	2.579	0.130	2.832	-0.587	3.251	--	--	--	--		--
S1522-1	0.204	4.926	0.0497	5.201	-0.259	5.651		Signal from microbarograph charge arrived				
-2	0.221	4.922	0.0507	5.207	-0.315	5.660		before crossover				
W51.8-1	4.82	0.730	1.17	0.949	-7.64	1.499	5.64	2.106	3.29	2.359	0.597	2.822
-2	4.34	0.729	1.07	0.956	-7.03	1.407	5.20	2.110	3.07	2.418	1.06	2.873
W108-1	2.48	0.982	0.613	1.131	-2.72	1.646	1.95	2.269	1.35	2.523	0.540	2.995
-2	2.40	0.978	0.586	1.132	-3.22	1.620	2.29	2.261	1.42	2.543	0.569	3.006
W259-1	0.851	1.406	0.159	1.552	-1.41	2.049	1.03	2.691	0.589	2.953	0.228	3.443
-2	0.835	1.411	0.152	1.549	-1.25	2.099	0.952	2.686	0.564	2.930	0.241	3.447
W460-1	0.490	1.989	0.108	2.154	-0.64	2.651	0.440	3.257	0.275	3.510	0.122	4.027
W701-1	0.322	2.690	0.080	2.864	-0.406	3.324	0.285	3.977	0.167	4.230	0.069	4.724
-2	0.333	2.687	0.083	2.860	-0.394	3.301	0.282	3.986	0.162	4.232	0.0695	4.730
W1039-1	0.215	3.662	0.0628	3.828	-0.278	4.325	0.184	4.934	0.135	5.170	0.0559	5.687
W1402-1	0.154	4.609	0.0307	4.765	-0.182	5.127	0.125	5.822	0.094	6.202	0.041	6.611
-2	0.158	4.602	0.0288	4.751	-0.193	5.110	0.125	5.824	0.102	6.123		

CH 5 - SUMMARY AND CONCLUSIONS

The Dugout detonation set up an air-blast wave train of three positive phases separated by two negative phases. A direct ground shock which should have had a velocity of about 4300 meters/second was not detected by arrival times, but peak overpressures suggest that it was still fairly strong at the closest gage station. A seismic surface wave with a velocity near 1600 meters/second was observed at all stations. Greatest peak overpressure came from a ground-shock-induced wave originated at the epicenter by the direct ground shock and propagated through the air at about 345 meters/second. Both waves are included in the first positive phase. The negative phase following the first positive phase was interrupted by superposition of a positive pulse from venting gases, which, because of the superposition on a negative wave had a lower than expected amplitude. After the long second negative phase, a compensating final positive pulse was apparently necessary to restore the air to ambient conditions.

The seismic surface wave propagated between the sonic velocity in soil and that in air, whereas the ground-shock-induced wave propagated near the velocity of sound in air, thus lengthening with increased distances the duration of the first positive phase. Peak overpressures attenuated with distance at a rate of $R^{-1.1}$, about the same as that measured for a single charge. Peak overpressures between 50 and 1000 m range from 1.39 times single-charge values along the west line (off the end) to 3.28 times those values along the south line (perpendicular). Thus, peak overpressures measured perpendicular to the row are about 65 percent those which would be obtained by multiplying single-charge overpressures by the number of charges. More precisely, off the end of a 5-charge row, single-charge peak overpressures are increased 10 percent for each charge (after the first) in the row; perpendicular to the row, the increase is 57 percent over single-charge values for each additional charge in the row. The ratio of peak overpressure from a row charge to peak overpressure from a single charge at these burial depths is approximately

$$\frac{P_{row}}{P_{single}} = n^{0.7}, \text{ perpendicular to the row}$$

and

$$\frac{P_{row}}{P_{single}} = n^{1/4}, \text{ off the end of the row.}$$

These expressions were derived from Dugout where the peaks from five charges were those from the ground-shock-induced pulse and from a smaller 11-charge row where the peaks appear to be those

from venting gases. Because of this difference in the dominant peaks, the consistency which permitted the above relationships may be shown by future experiments to be coincidental.

Peak overpressures perpendicular to the row are a little more than twice those measured off the end.

In general, all subsequent waves were attenuated with distance at about $R^{-1.1}$. Peaks of the subsequent phases measured perpendicular to the row were twice those measured off the end except for that of the first negative phase, which could not be determined, and that of the second negative phase, which was about 50 percent greater.

Peak overpressure differences because of the terrain profile along the west blast line were small-deduced from shock tube experiments to be less than +10, -5 percent of level terrain values. Differences this small are not detectable within the scatter of the data.

Phase impulses also attenuated with distance as $R^{-1.1}$ except for the last positive phase, which was attenuated at a smaller rate, and the first negative phase, for which a rate could not be determined. Only in the case of the first positive-phase impulse were the values larger perpendicular to the row than along the axis of the row, in which case they were 50 percent larger.

Except for the first positive phase, for which the duration was increased with distance because of the different propagation rates of the two waves, the durations were relatively constant with distance.

APPENDIX A

Auxiliary Figures

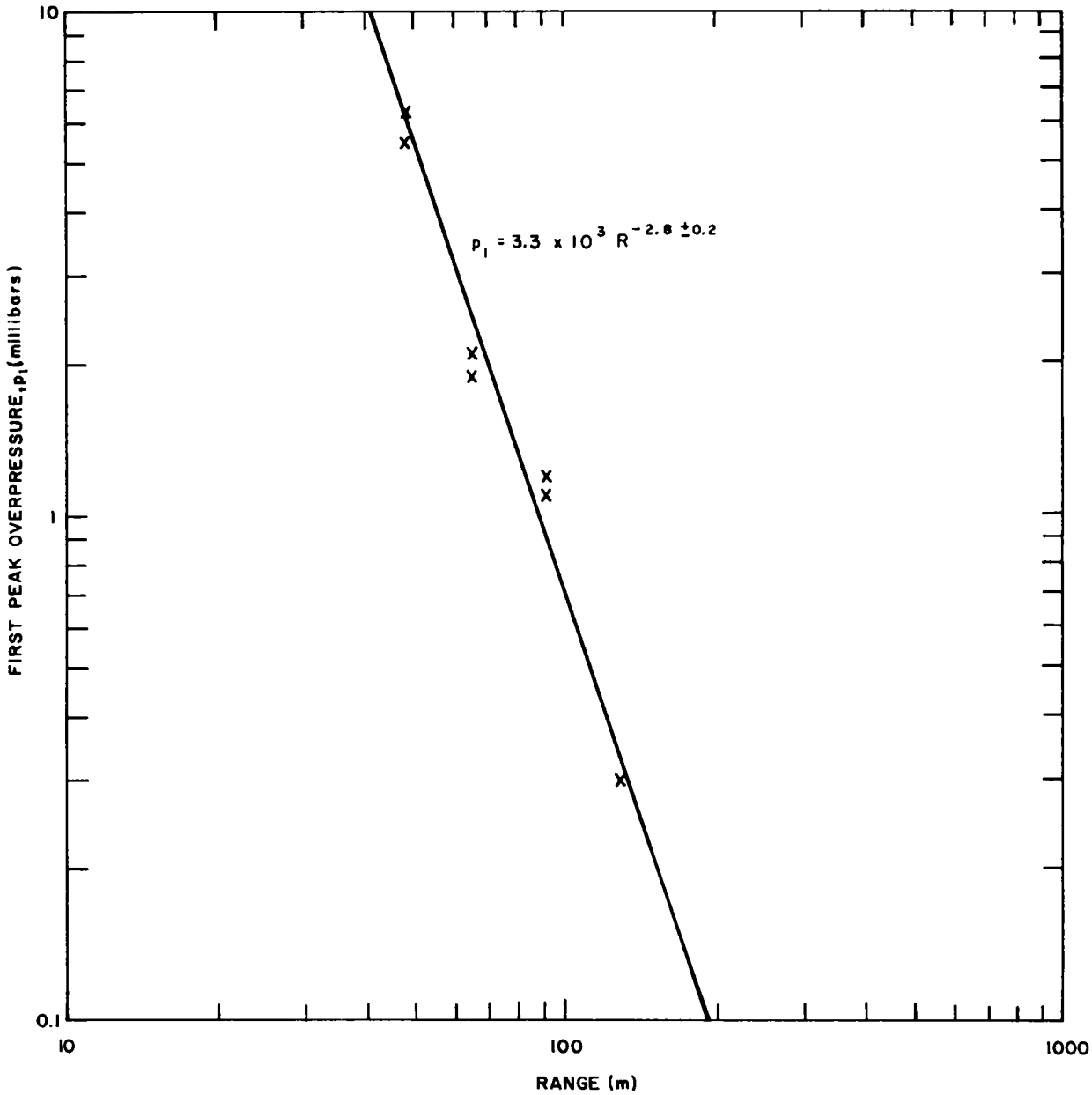

Figure A.1. Buckboard results--first peak overpressure versus range ($p_1 = 3.3 \times 10^3 R^{-2.8 \pm 0.2}$)

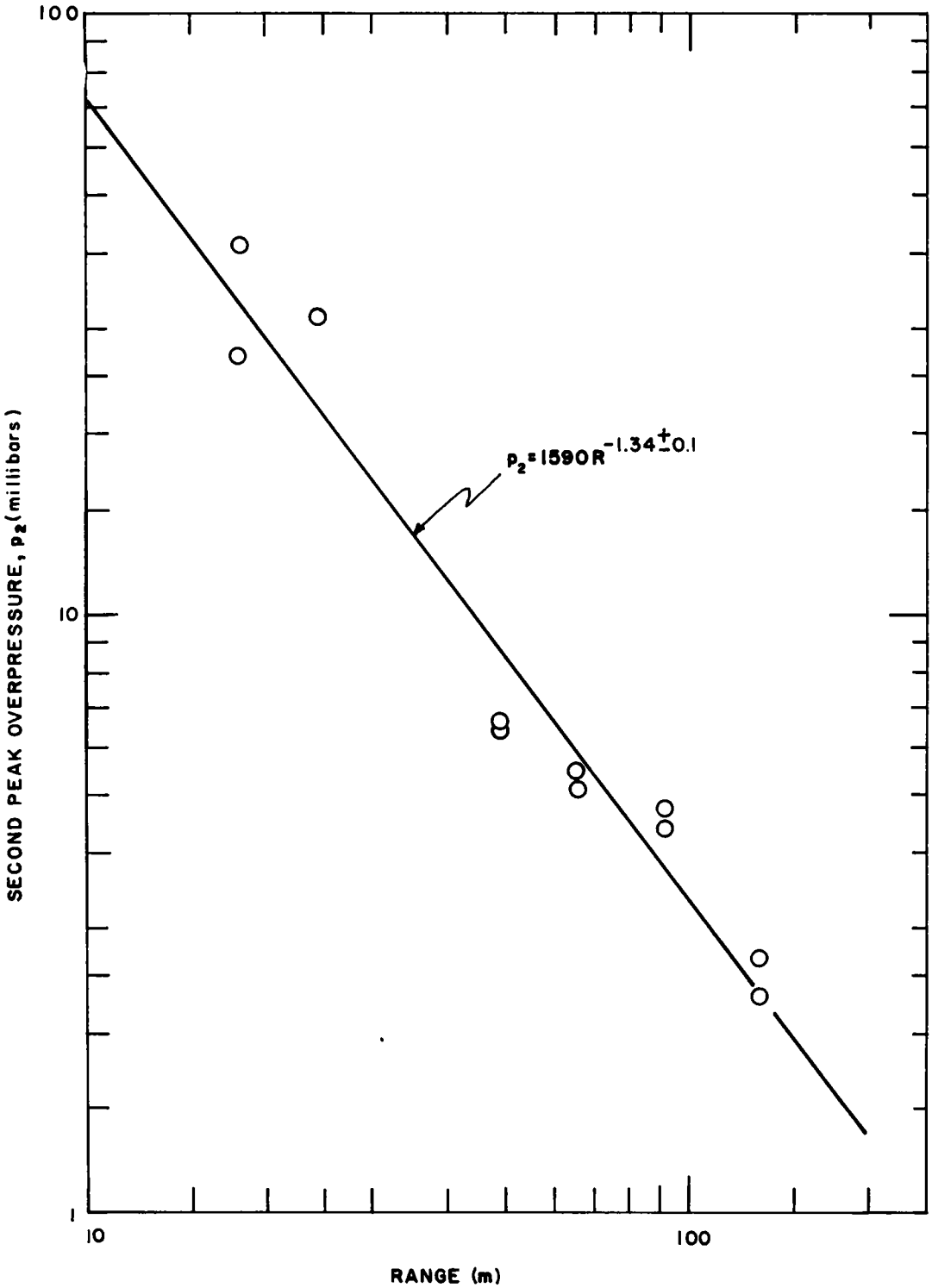

Figure A.2. Buckboard results--second peak overpressure versus range ($P_2 = 1590\ R^{-1.34 \pm 0.1}$)

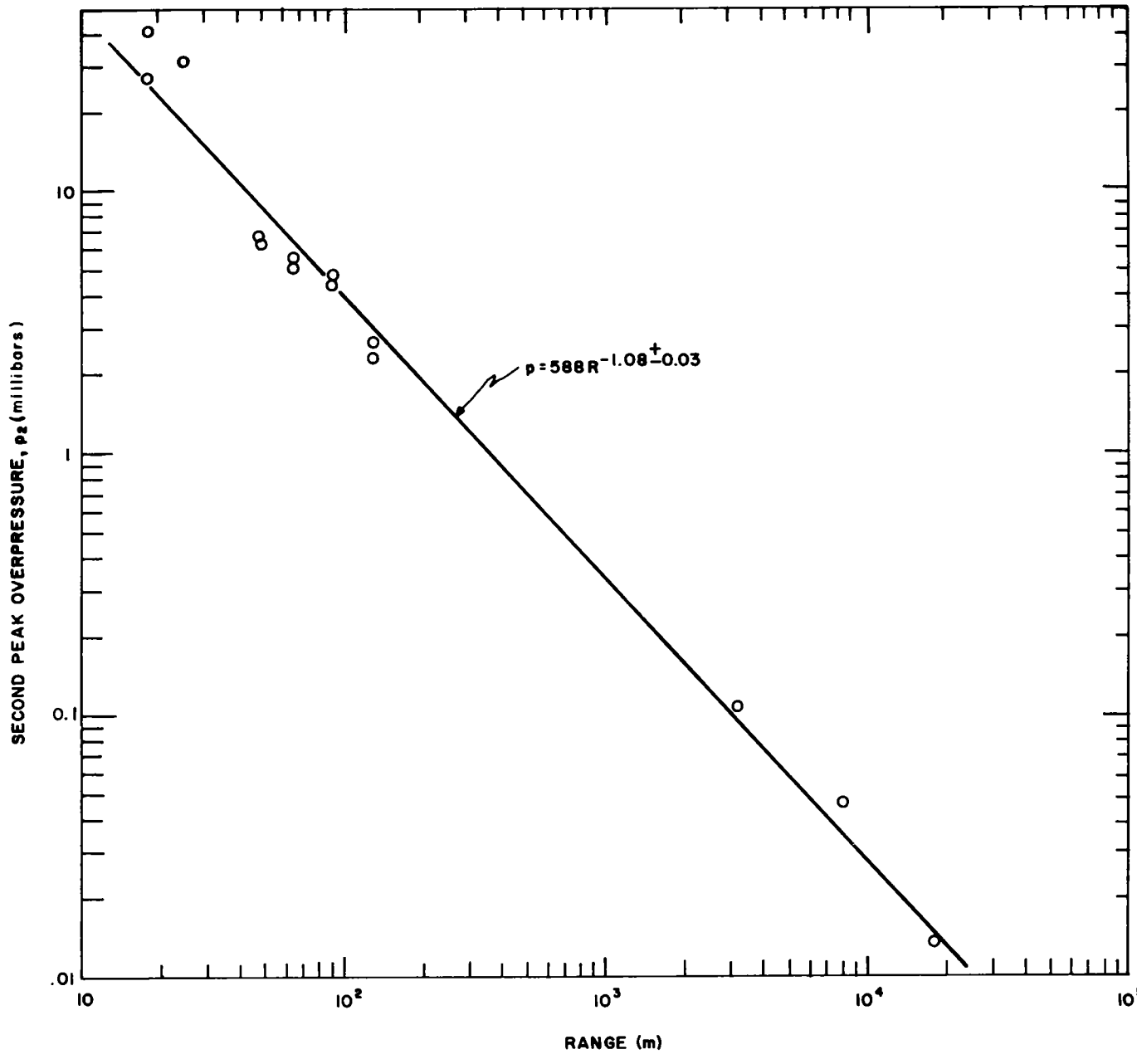

Figure A.3. Buckboard results--second peak overpressure ($p = 588\, R^{-1.08 \pm 0.03}$)

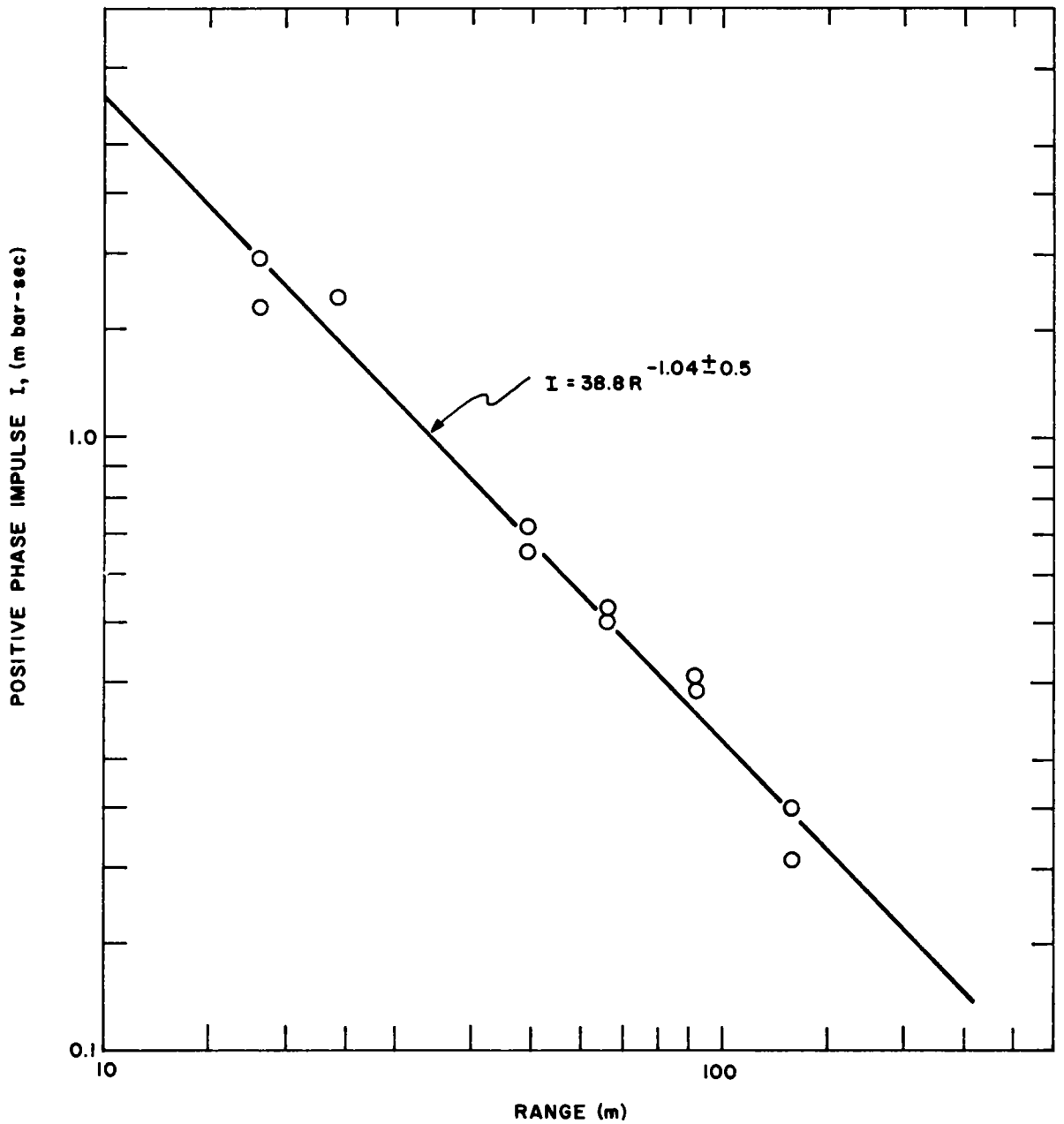

Figure A.4. Buckboard results--positive-phase impulse versus range

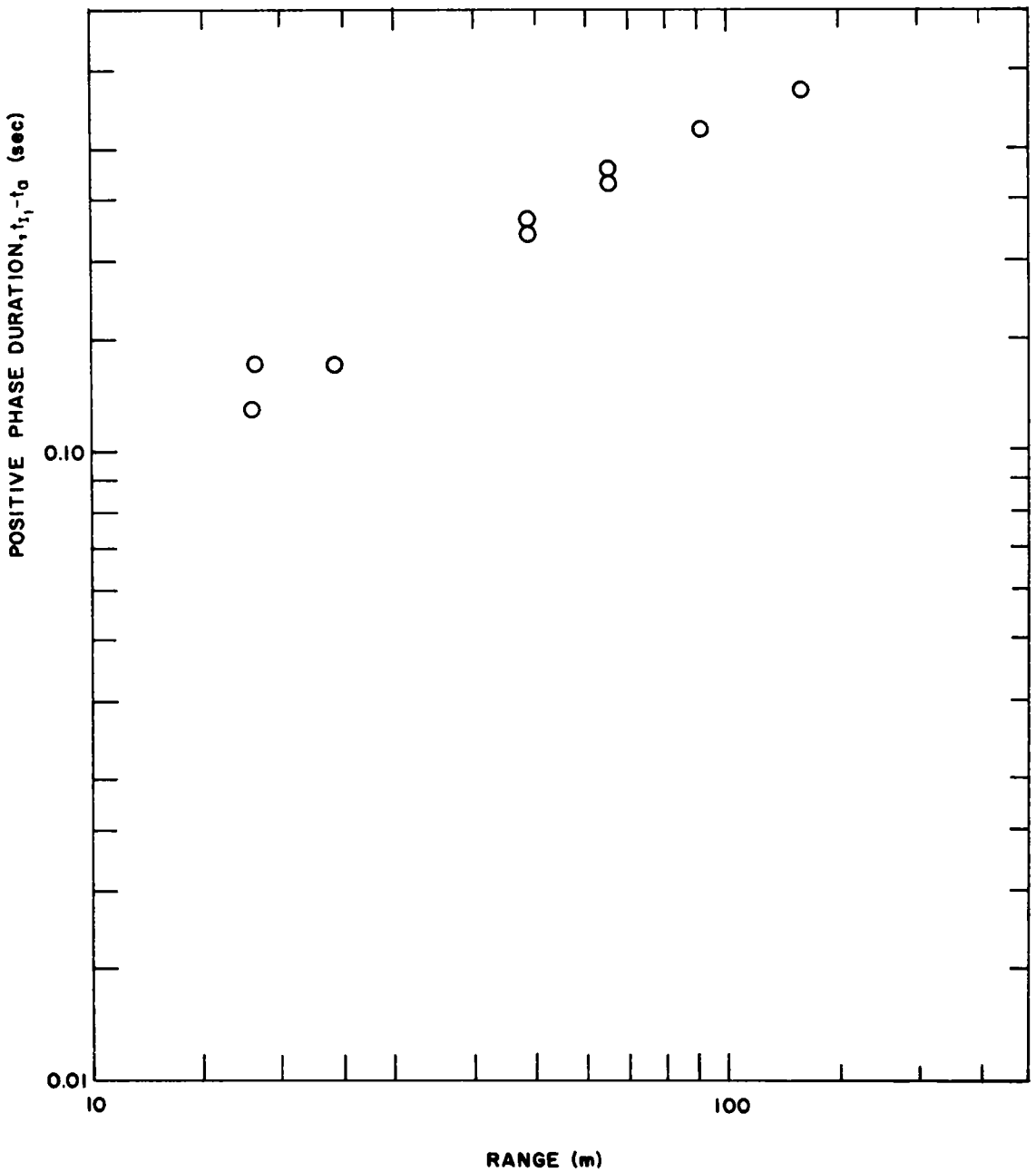

Figure A.5. Buckboard results--positive-phase duration versus range

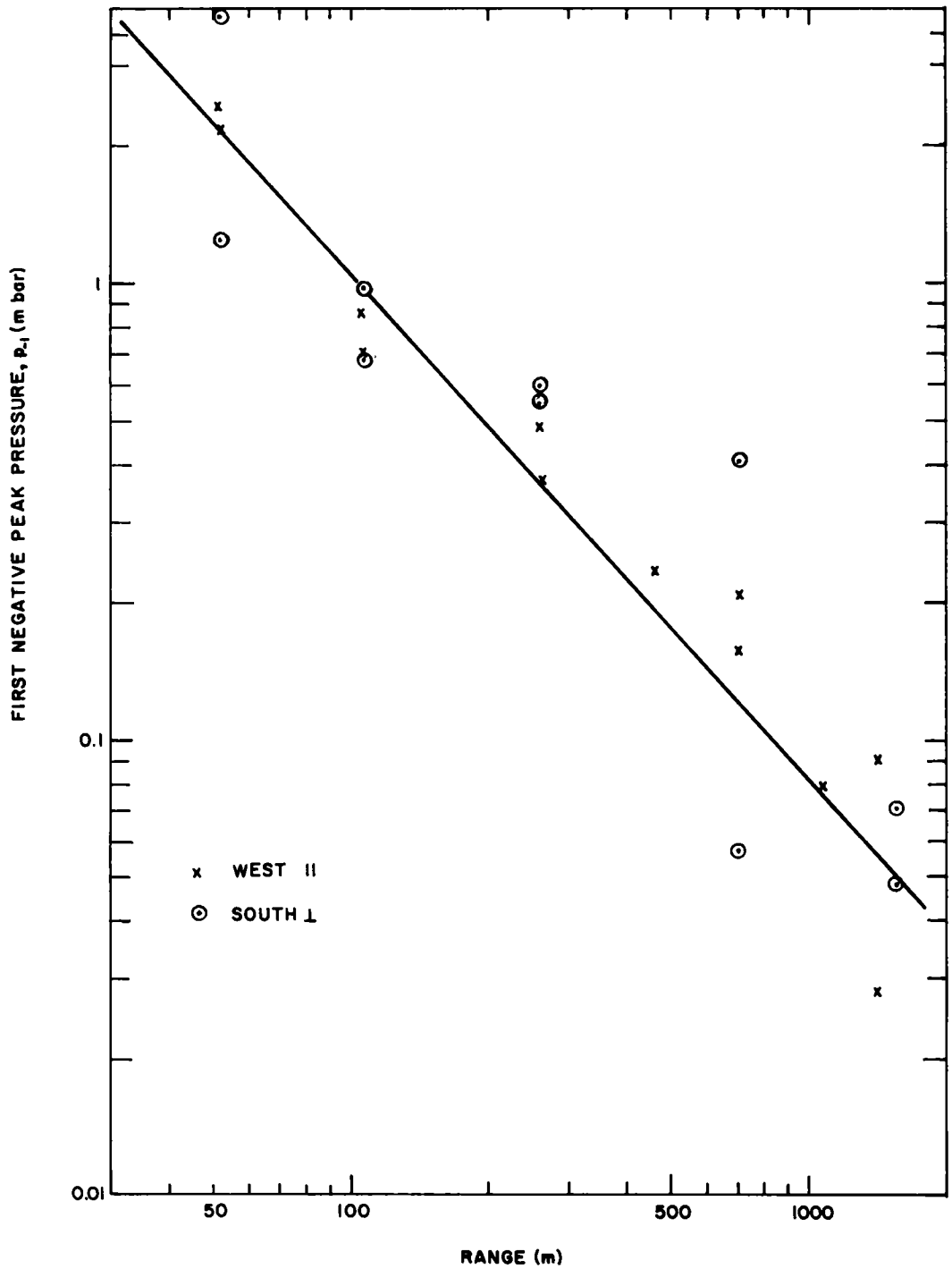

Figure A.6. First negative peak pressure

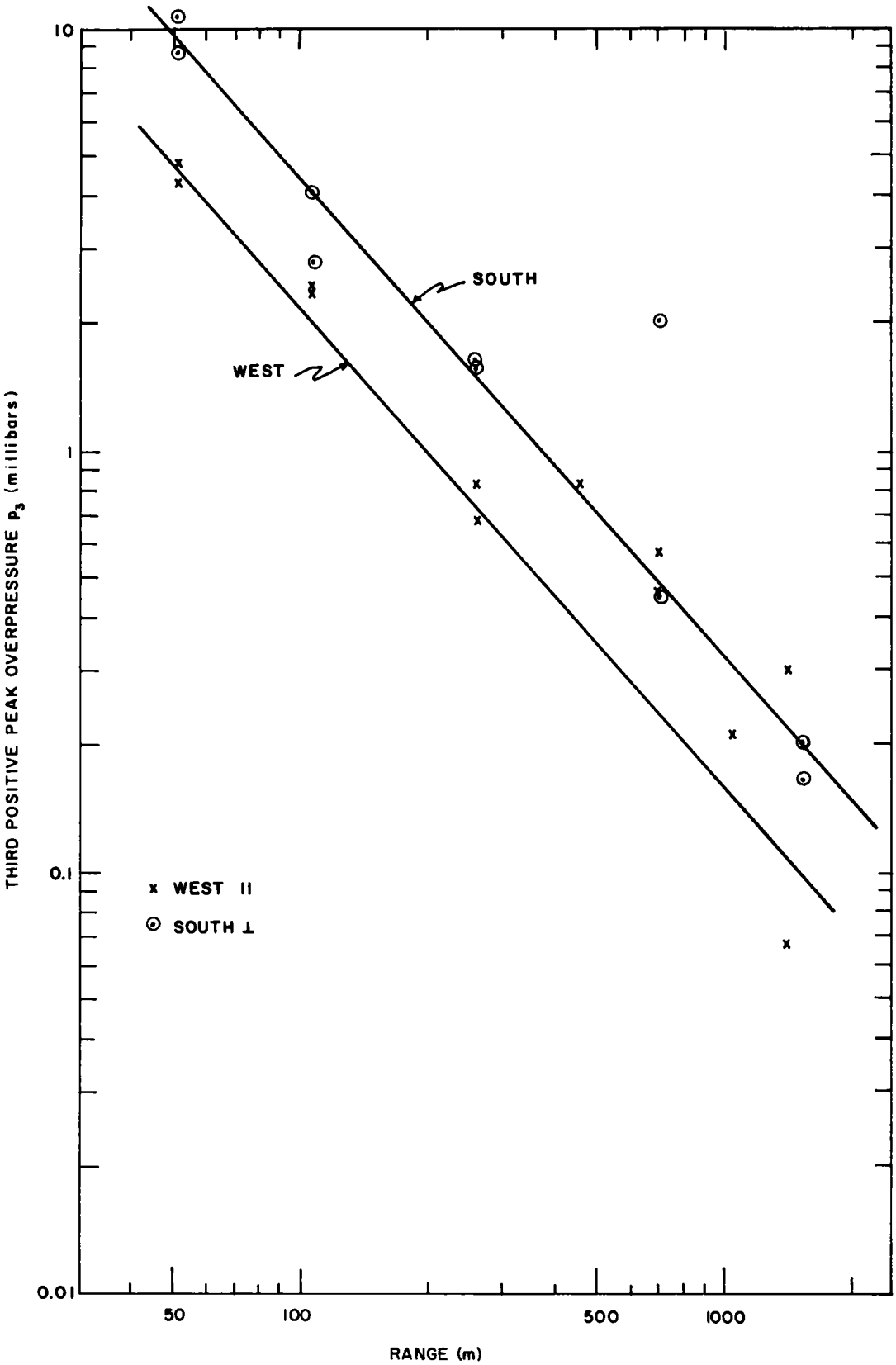

Figure A.7. Third positive peak overpressure

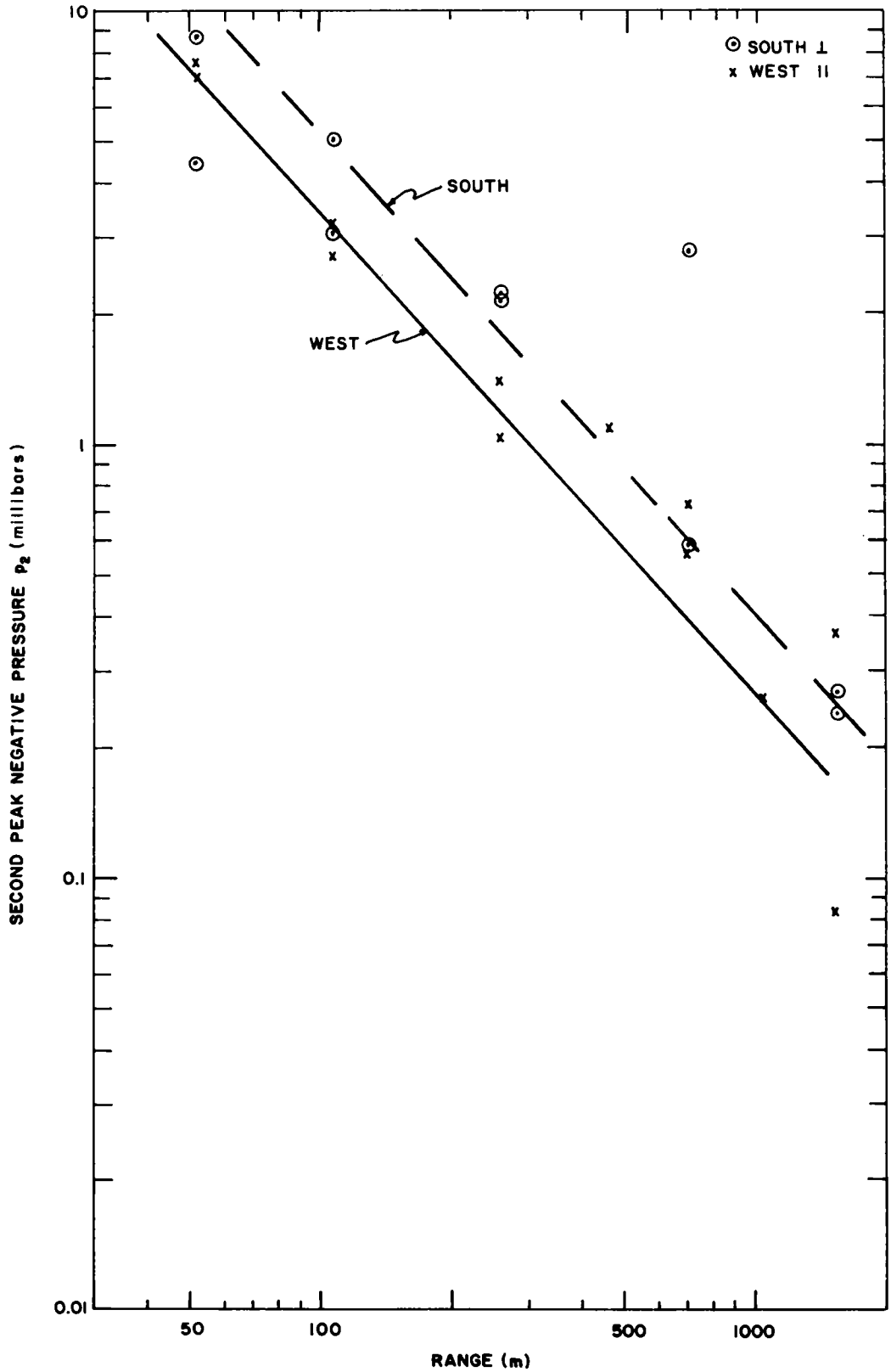

Figure A.8. Second negative peak overpressure

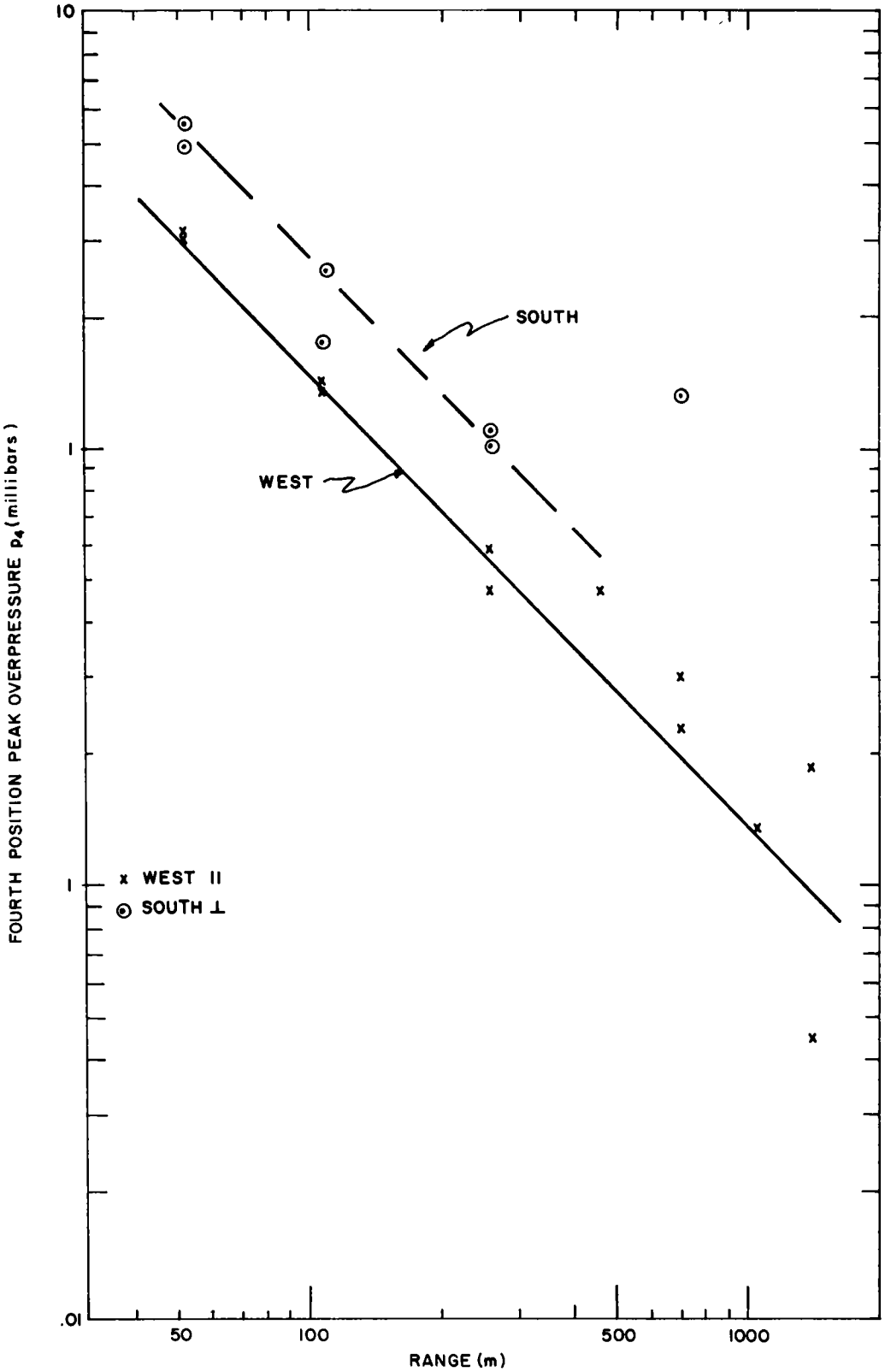

Figure A.9. Fourth positive peak overpressure

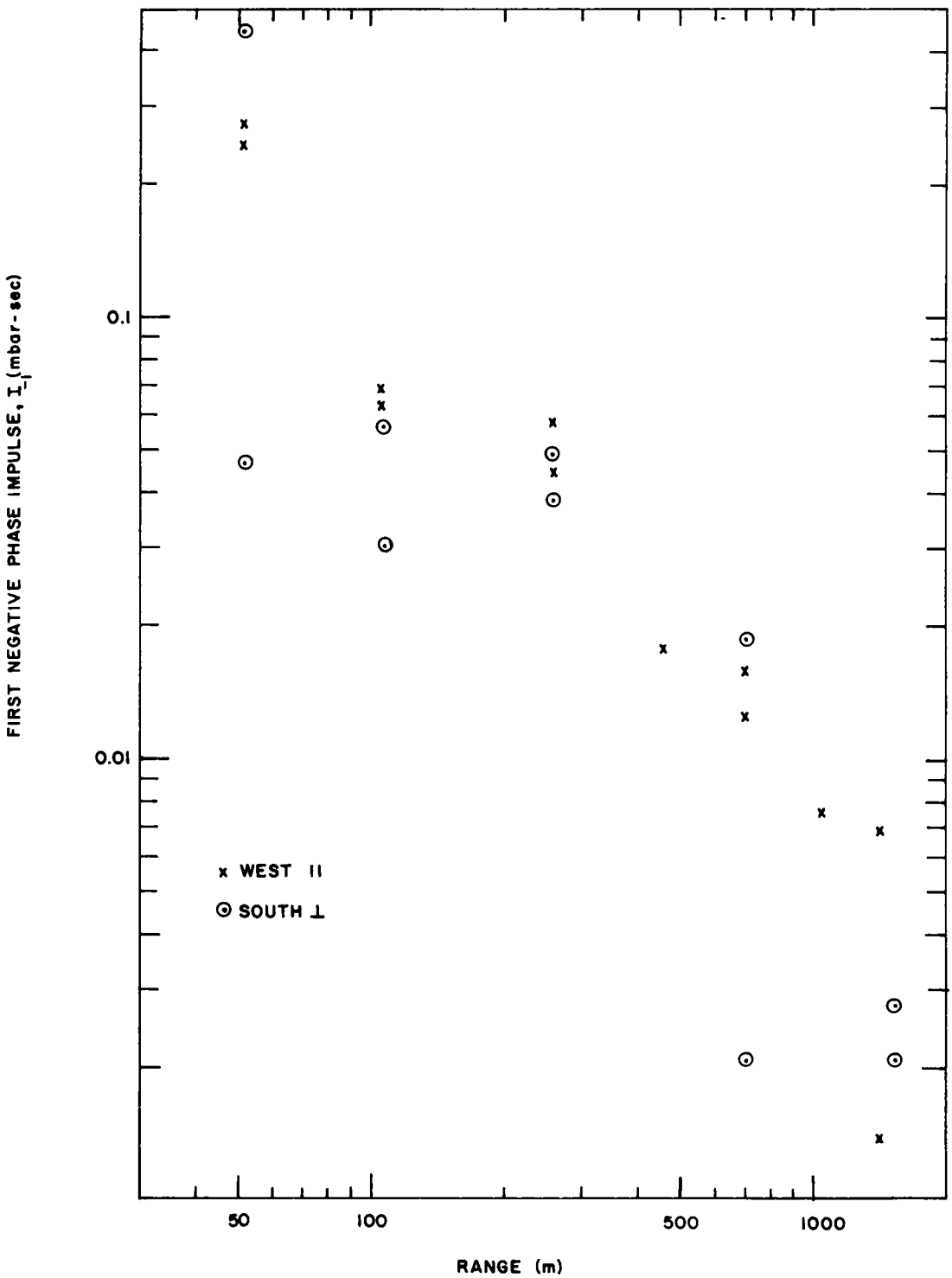

Figure A.10. First negative-phase impulse

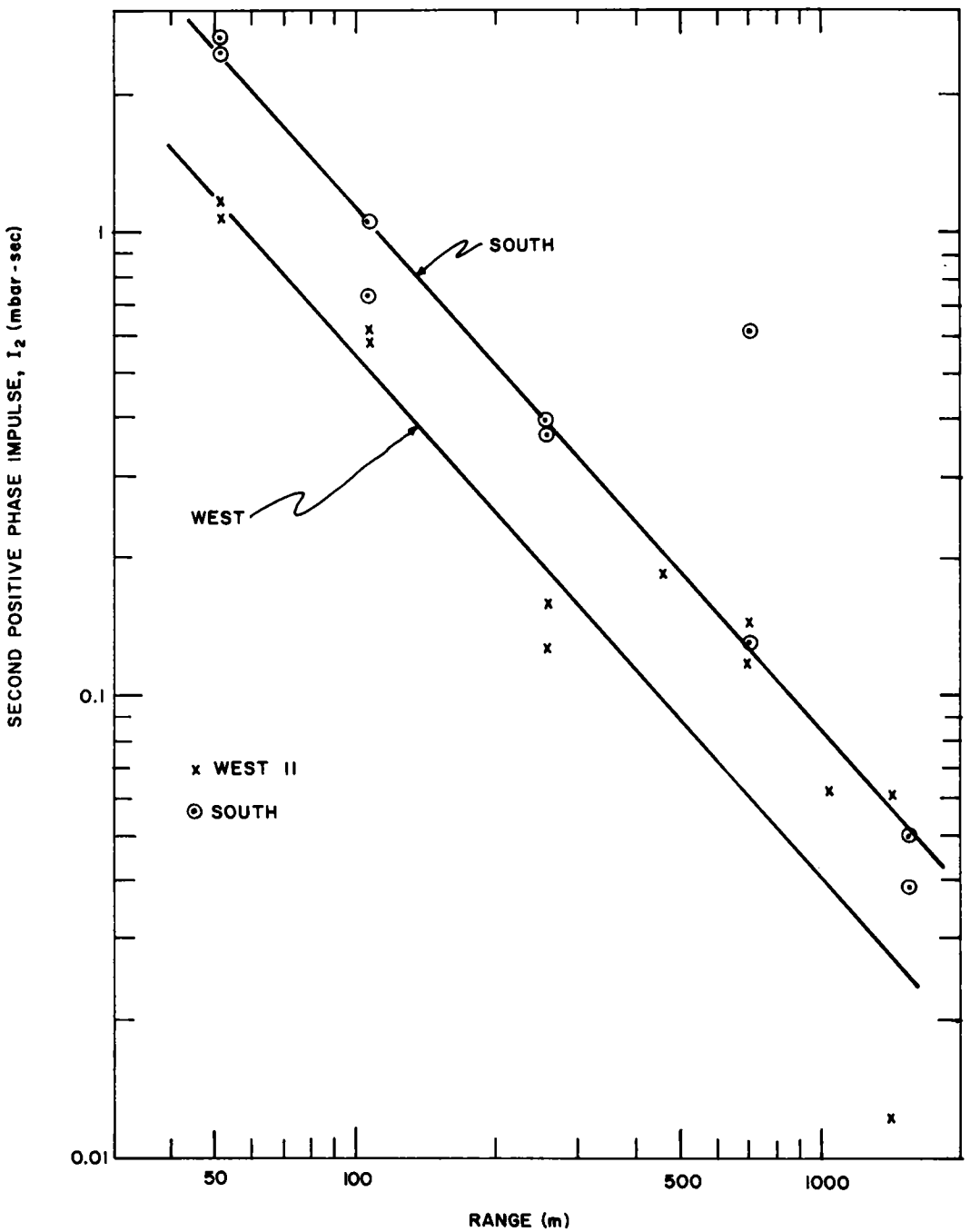

Figure A.11. Second positive-phase impulse

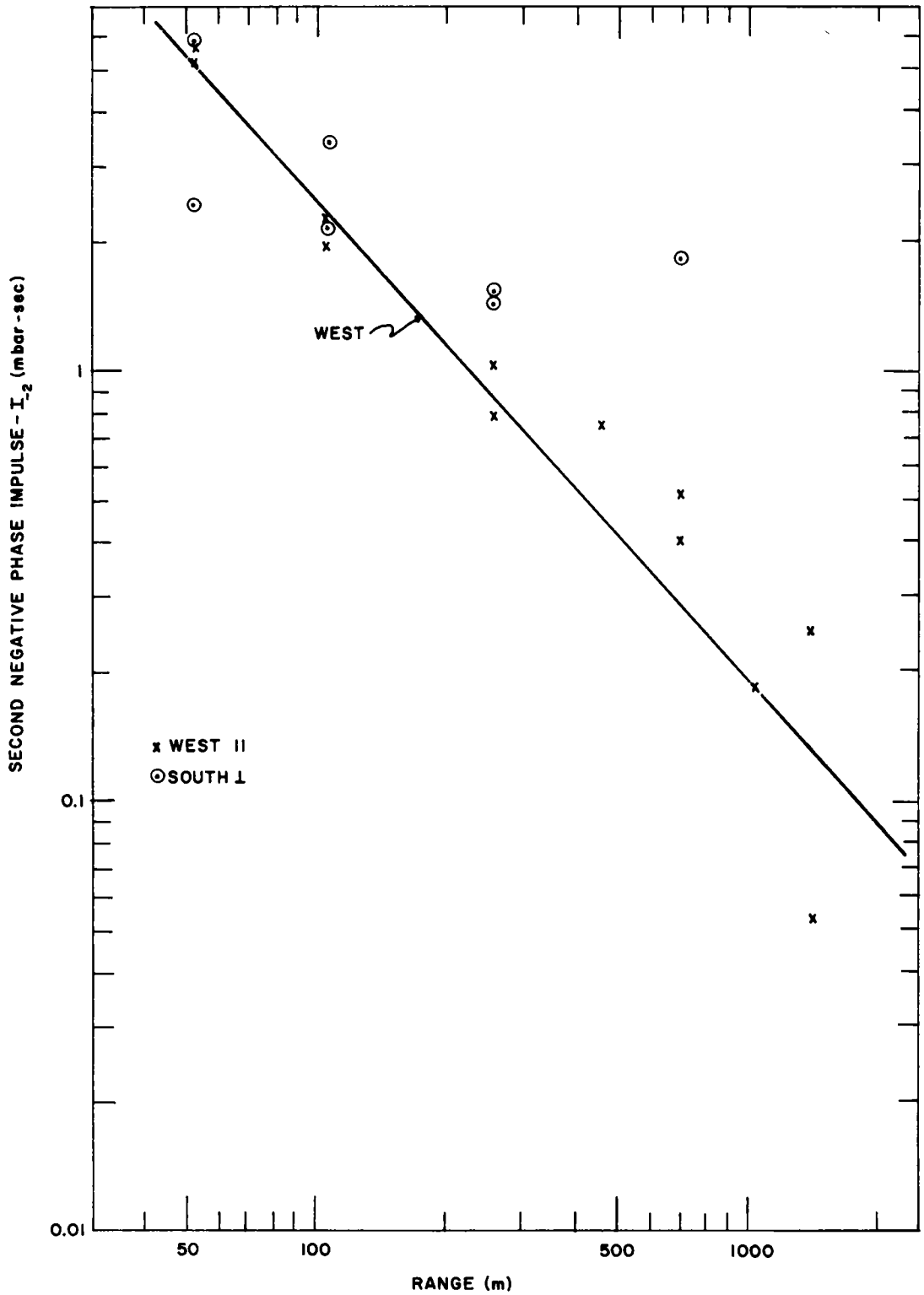

Figure A.12. Second negative-phase impulse

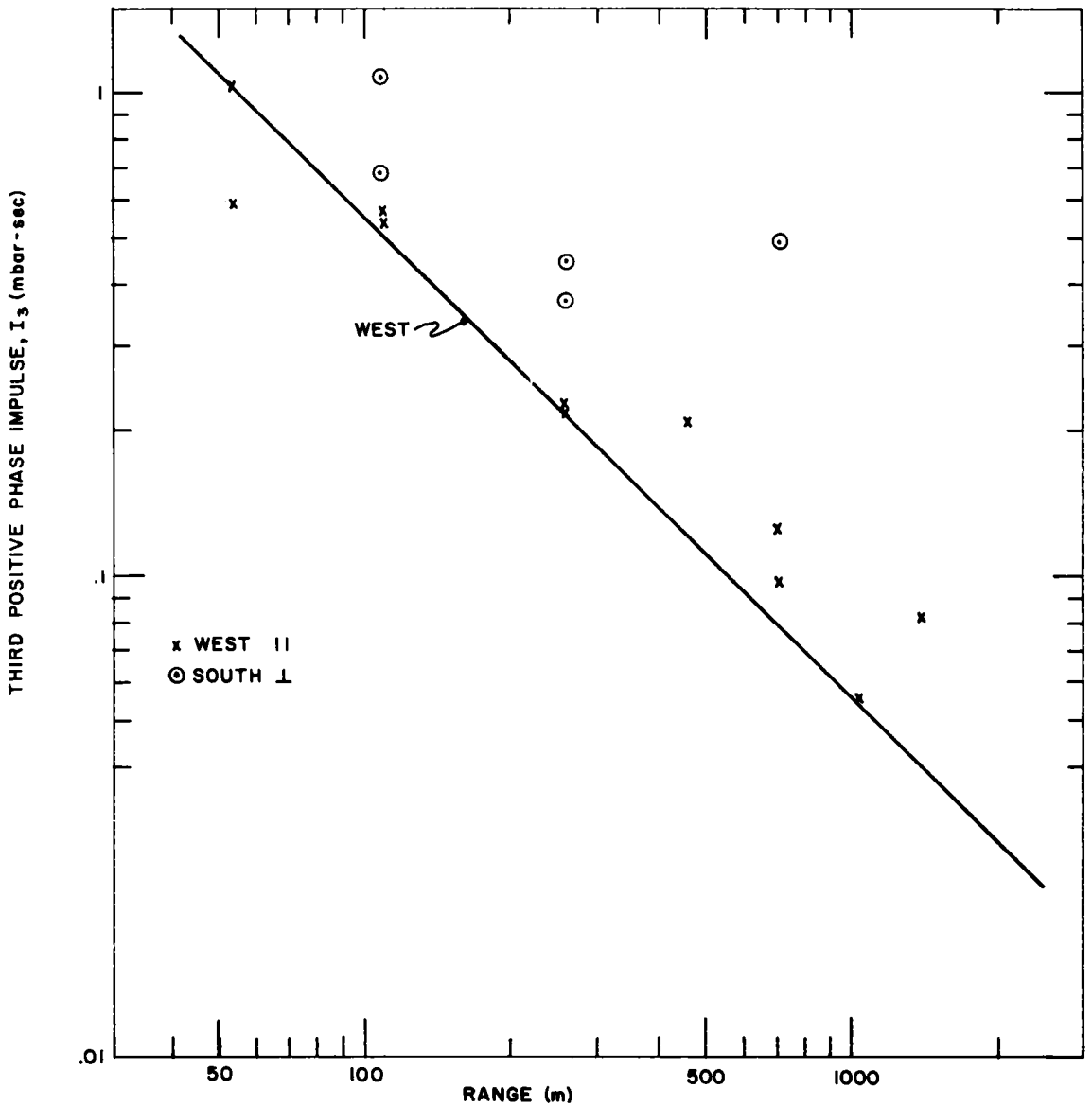

Figure A.13. Third positive-phase impulse

REFERENCES

1. Brinkley, S. R., Jr., and Kirkwood, J. G., The Blast Wave in Air Produced by Line Charges, NRDL Report No. A-343, OSRD Report No. 5659, October 4, 1945.

2. Adams, C. L., et al, Comparison of the Blast from Explosive Charges of Different Shapes, Ballistic Research Laboratories Report No. 681, January 1949.

3. Fraenkel, G. K., and Kennedy, W. D., Air Blast from Line Charges, NRDL Report No. A-375, OSRD Report No. 6253, March 15, 1946.

4. Perret, W. R., et al, Project Scooter, Final Report, SC-4602(RR), October 1963.

5. Vortman, L. J., et al, 20-Ton HE Cratering Experiments in Desert Alluvium, Project Stagecoach, Final Report, SC-4596(RR), May 1962.

6. Vortman, L. J., et al, 20-Ton and 1/2-Ton High Explosive Cratering Experiments in Basalt Rock, Project Buckboard, Final Report, SC-4675(RR), Sandia Corporation, November 1960.

7. Unpublished data; Sandia Corporation tests, 1962.

8. Nordyke, M. D., Summary of Results from Rowboat, UCRL Memorandum 8, February 14, 1962.

9. Graves, E., Wray, W. R., and Pierce, R. B., Scope of Chemical Explosive Cratering Experiment, Project Pre-Buggy Preliminary Report, PNE-300, August 1963.

10. Spruill, J. L., "The Pre-Buggy Chemical Cratering Experiments," Undated memorandum, Nuclear Cratering Group.

11. Ingram, L. F., Earth-Motion Measurements, POR-1811 (WT-1811) Project Danny Boy Final Report, Waterways Experiment Station, November 20, 1964.

12. Carder, Bruce M., Surface Phenomena Photography, POIR-1812 (ITR-1812), Project Danny Boy Preliminary Report, Edgerton, Germeshausen & Grier, Inc., February 15, 1963.

13. Johnson, G. W., and Higgins, G. H., Engineering Applications of Nuclear Explosives: Project Plowshare, UCRL-7634, Lawrence Radiation Laboratory, May 19, 1964.

14. Knox, Joseph B., Lawrence Radiation Laboratory, personal communication.

15. Nordyke, Milo D., Lawrence Radiation Laboratory, personal communication.

16. Kingery, C. N., and Pannill, B. F., Peak Overpressure vs Scaled Distance for TNT Surface Bursts (Hemispherical Charges), Ballistic Research Laboratories Memorandum Report No. 1518, April 1964.

17. Merritt, M. L., Air Shock Pressures as Affected by Hills and Dales, Operation Tumbler-Snapper, WT-502, September 15, 1952.

18. Merritt, M. L., Air Shock Pressures as Affected by Hills and Dales, Operation Upshot-Knothole, WT-713, March 13, 1954.

19. Bryant, E. J., and Keefer, J. H., Effects of Rough and Sloping Terrain on Blast Wave, Operation Plumbbob, WT-1407, Ballistic Research Laboratory.

20. Todd, J., Jr., A Scale Model Study of the Effects of Symmetric Ridges on Blast Overpressures, SC-3335 (TR), Sandia Corporation, May 3, 1954.

DUGOUT TECHNICAL REPORTS

Report No.	Agency	Author	Title
PNE-600F	LRL	Nordyke, et al.	Technical Director's Summary Report – Project Dugout
PNE-601F	NCG	Spruill	Apparent Crater Studies
PNE-602F	WES	Strohm	Crater Explorations
PNE-603F*	LRL	Terhune	Surface Motion Measurements
PNE-604F	LRL	Rohrer	Cloud Development
PNE-605F	CGS	Mickey	Strong Motion Measurements
PNE-607F	SC	Reed	Multiple Row Charge Blast Wave Observations at Long Range
PNE-608F	SC	Vortman	Close-in Air Blast From a Row Charge in Basalt
PNE-609F	WES	Ingram	Deep Underground Shock Measurements

*PNE-603F and PNE-606F incorporated under one document number per request of Milo Nordyke.